DÜZCE ÜNİVERSİTESİ | LİSANSÜSTÜ EĞİTİM ENSTİTÜSÜ

INVESTIGATING OPTİCAL PROPERTIES OF ZINC DOPED PEROVSKITE QUANTUM DOTS AND QLED APPLICATIONS

ELİF YALVA

YÜKSEK LİSANS TEZİ
ELEKTRİK VE BİLGİSAYAR MÜHENDİSLİĞİ
DİSİPLİNLERARSI ANABİLİM DALI

DANIŞMAN

DOÇ. DR. MUSA ÇADIRCI

DÜZCE,2024

T.C.
DÜZCE ÜNİVERSİTESİ
LİSANSÜSTÜ EĞİTİM ENSTİTÜSÜ

SYNTHESIS OF SEMICONDUCTOR PEROVSKITE QUANTUM DOTS AND QLED APPLICATIONS

Elif YALVA tarafından hazırlanan tez çalışması aşağıdaki jüri tarafından Düzce Üniversitesi Lisansüstü Eğitim Enstitüsü Elektrik ve Bilgisayar Mühendisliği Disiplinlerarası Anabilim Dalı'nda **YÜKSEK LİSANS TEZİ** olarak kabul edilmiştir.

Tez Danışmanı

Doç. Dr. Musa ÇADIRCI

Düzce Üniversitesi

Jüri Üyeleri

Doç. Dr. Musa ÇADIRCI
Düzce Üniversitesi _____

Doç. Dr. Erdem ELİBOL
Düzce Üniversitesi _____

Doç. Dr. Ali Al-Otaify
Qassim Üniversitesi _____

Yedek Jüri Üyeleri

Doç. Dr. Emre Çelik
Düzce Üniversitesi _____

Doç. Dr. Yasemin Gündoğdu
Selçuk Üniversitesi _____

Tez Savunma Tarihi: 04/07/2024

BEYAN

Bu tez çalışmasının kendi çalışmam olduğunu, tezin planlanmasından yazımına kadar bütün aşamalarda etik dışı davranışımın olmadığını, bu tezdeki bütün bilgileri akademik ve etik kurallar içinde elde ettiğimi, bu tez çalışmasıyla elde edilmeyen bütün bilgi ve yorumlara kaynak gösterdiğimi ve bu kaynakları da kaynaklar listesine aldığımı, yine bu tezin çalışılması ve yazımı sırasında patent ve telif haklarını ihlal edici bir davranışımın olmadığını beyan ederim.

Elif YALVA

TEŞEKKÜR

Yüksek Lisans öğrenimim sırasında ve bu tezin hazırlanmasında gösterdiği her türlü destek ve yardımdan dolayı, çok değerli hocam Doç. Dr. Musa ÇADIRCI Beye en içten dileklerimle teşekkür ederim.

Bu çalışma boyunca yardımlarını ve desteklerini esirgemeyen sevgili aileme ve çalışma arkadaşlarıma sonsuz teşekkürlerimi sunarım.

04.06.2024 Elif YALVA

TABLE OF CONTENTS

FIGURE LIST

ABBREVIATIONS

QDs	Quantum Dots
LEDs	Light Emitting Diode
PQDs	Perovskite Quantum Dots
QLED	Quantum Light Emitting Diode
PQLED	Perovskite Quantum Light Emitting Diode
OLED	Organic Light Emitting Diode
GPVDM	Generalized Photovoltaic Device Model
PLQY	Photoluminescence Quantum Yield
NBE	Near Band Edge
HIL	Hole Injection Layer
HTL	Hole Transfer Layer
QW	Quantum Well
LUMO	Lowest Unoccupied Molecular Orbital
HOMO	Highest Unoccupied Molecular Orbital
ODE	Octadecene
OA	Oleic Acid
OLA	Oleyl Amine
ZnO	Zinc Oxide
LiF	Lithium Floride
PL	Photoluminescence
FWHM	Full Width Half Maximum

ÖZET

Elif YALVA

Düzce Üniversitesi

Lisansüstü Eğitim Enstitüsü, Elektrik ve Bilgisayar (Disiplinlerarası) Mühendisliği Anabilim Dalı Yüksek Lisans Tezi

Danışman: Doç. Dr. Musa

ÇADIRCI

Temmuz 2024, 50 sayfa

Bu tez, sezyum kurşun halojenür ($CsPb(ClBr)_3$) kuantum noktalarının (QD'ler) optik özellikleri ve cihaz performansı üzerine kapsamlı bir araştırma sunmaktadır, çinko (Zn) katkılamanın etkileri üzerine odaklanmaktadır. Çalışma, Zn katkılı $CsPb(ClBr)_3$ QD'lerin fotolüminesans (PL) ve UV-Vis soğurma spektrumlarını sistematik olarak inceleyerek, katkılama konsantrasyonunun optik kararlılık üzerindeki etkisini ortaya koymaktadır. Bulgular, Zn katkılamanın QD'ların dayanıklığını artırarak PL ve soğurma özelliklerini iyileştirdiğini göstermektedir. Özellikle, zaman bağımlı soğurma ve PL davranışı, kararlı optik performans gerektiren uygulamalar için katkılama oranlarını ve zamansal etkileri dikkate almanın önemini vurgulamaktadır. Ek olarak, bu çalışma OghmaNano (GPVDM) programı kullanılarak kuantum nokta ışık yayan diyot (QLED) cihazlarının simülasyonu incelenmiştir. Çalışma, aktif tabaka kalınlığı ve bir boşluk enjeksiyon tabakasının (LiF) dahil edilmesi gibi cihaz parametrelerinin, akım-gerilim karakteristikleri, verimlilik ve ışık yayma gibi temel performans ölçütleri üzerindeki etkisini incelemektedir. Sonuçlar, QLED cihaz tasarımının optimize edilmesi ve GPVDM simülasyon aracının yeteneklerinden yararlanılması için önemli bilgiler sağlamaktadır.

Anahtar Kelimeler: Perovskit kuantum nokta, QLED uygulamaları

ABSTRACT

Elif YALVA

Düzce University

Graduate Education Institute, Department of Electrical and Computer Engineering

(Interdisciplinary) Master Thesis

Thesis Supervisor: Associate Professor Musa ÇADIRCI

July 2024, 50 pages

This thesis presents a comprehensive investigation into the optical properties and device performance of cesium lead halide ($CsPb(ClBr)_3$) quantum dots (QDs), with a focus on the effects of zinc (Zn) doping. The study systematically examines the photoluminescence (PL) and UV-Vis absorbance spectra of Zn-doped $CsPb(ClBr)_3$ QDs over time, revealing the influence of doping concentration on optical stability. The findings indicate that Zn doping enhances the monodispersity and charge carrier confinement of the QDs, leading to improved PL and absorbance characteristics. Notably, the time-dependent absorbance and PL behavior underscore the importance of considering doping ratios and temporal effects for applications requiring stable optical performance. Additionally, this work explores the simulation of quantum dot light-emitting diode (QLED) devices using the OghmaNano (GPVDM) program. The study examines the impact of device parameters, such as active layer thickness and the inclusion of a hole injection layer (LiF), on key performance metrics like current-voltage characteristics, efficiency, and light emission. The results provide valuable insights for optimizing QLED device design and leveraging the capabilities of the GPVDM simulation tool.

Keywords: Perovskite Quantum Dots, QLED Applications

1.INTRODUCTION

1.1. Quantum Dots

In nanotechnology, QDs are extraordinary semiconductor nanoparticles with unique optical and electronic characteristics. These nanoparticles, ranging from 2 to 10 nanometers, exhibit quantum mechanical properties, making them versatile candidates for various applications across multiple fields [1]. Due to quantum confinement effects, QDs demonstrate remarkable optical and electronic properties at the nanoscale. As seen in Figure 1.1, QDs can be in the core-only or core-shell structure, along with ligands at the surface, stabilizing them.

Unlike bulk materials, the electronic behavior of QDs is significantly influenced by their size and composition. QDs exhibit a phenomenon known as quantum confinement, where the electronic energy levels become discrete due to the spatial confinement of charge carriers within the nanoparticle, as seen in Figure 1.2. As a result, QDs can emit light at specific wavelengths determined by their size and composition. These tunable emission spectra enable the customization of emitted light, making QDs ideal for various applications requiring precise control over optical properties. Furthermore, QDs possess high photoluminescence quantum yields, indicating their efficiency in converting absorbed light into emitted photons. This property is crucial for applications such as light-emitting diodes (LEDs) and displays, where bright and vibrant colors are desired. Additionally, QDs exhibit exceptional photostability, retaining their optical properties over prolonged periods, making them suitable for long-term applications [2].

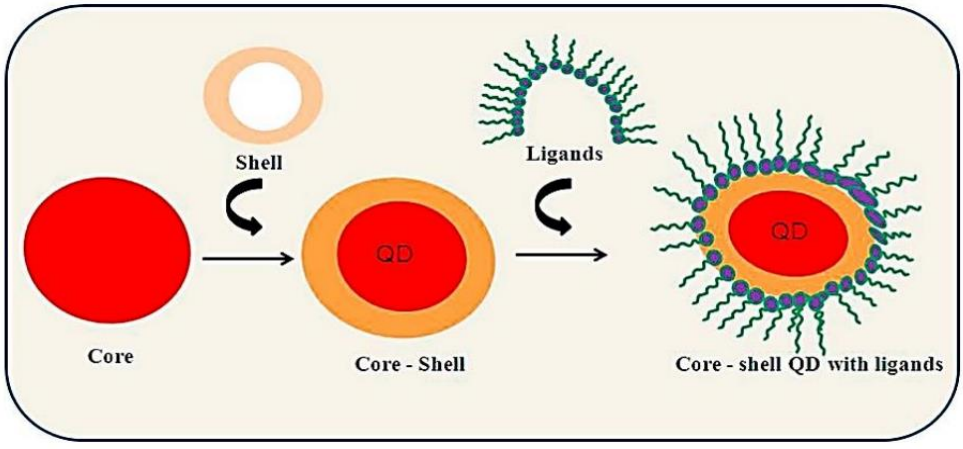

Figure 1.1. Schematic Representation of Quantum Dot Structure [7]

Several techniques have been developed for synthesizing QDs with precise size, shape, and composition control. One standard method involves the colloidal synthesis of QDs using chemical precursors in a solution-phase reaction. Typically, this method involves the injection of a precursor solution containing materials such as cadmium or lead into a hot solvent, where nucleation and growth of QDs occur under controlled conditions. The size and properties of the resulting QDs can be finely tuned by adjusting reaction parameters such as temperature, precursor concentration, and reaction time [3]. Alternatively, epitaxial growth techniques, such as molecular beam epitaxy (MBE) and metalorganic chemical vapor deposition (MOCVD), can fabricate QDs on crystalline substrates with atomic precision. These techniques offer superior control over the structural and compositional properties of QDs, making them particularly suitable for integrated optoelectronic devices [4].

One of the critical advantages of QDs lies in their tunable emission spectra, which enable precise control over the wavelength of emitted light. By simply adjusting the size, composition, or surface chemistry of QDs, researchers can tailor their optical properties to meet specific application requirements. This tunability makes QDs ideal candidates for various optoelectronic devices, including LEDs, displays, and solar cells. Another advantage of QDs is their high photoluminescence quantum yield, indicating their efficiency in converting absorbed photons into emitted light. This property is crucial for applications requiring bright and vibrant colors, such as display technologies and biomedical imaging. Furthermore, QDs exhibit exceptional photostability, retaining their optical properties over prolonged periods, even under harsh environmental conditions. This longevity makes them suitable for long-term applications in outdoor displays, lighting, and sensing devices [5]. From display technologies and biomedicine to solar energy harvesting, QDs have demonstrated their potential to revolutionize diverse industries. Continued research and development in synthesis methods, device fabrication, and application integration are poised to unlock further advancements and commercialization opportunities for quantum dot-based technologies, paving the way for a brighter and more sustainable future [6]. QDs are made of various materials, including cadmium selenide, lead sulfide, indium arsenide, copper selenide, perovskite QDs, etc.

Each type of QD has unique properties and, hence, application areas. Among them, perovskite QDs show great potential for optoelectronic applications.

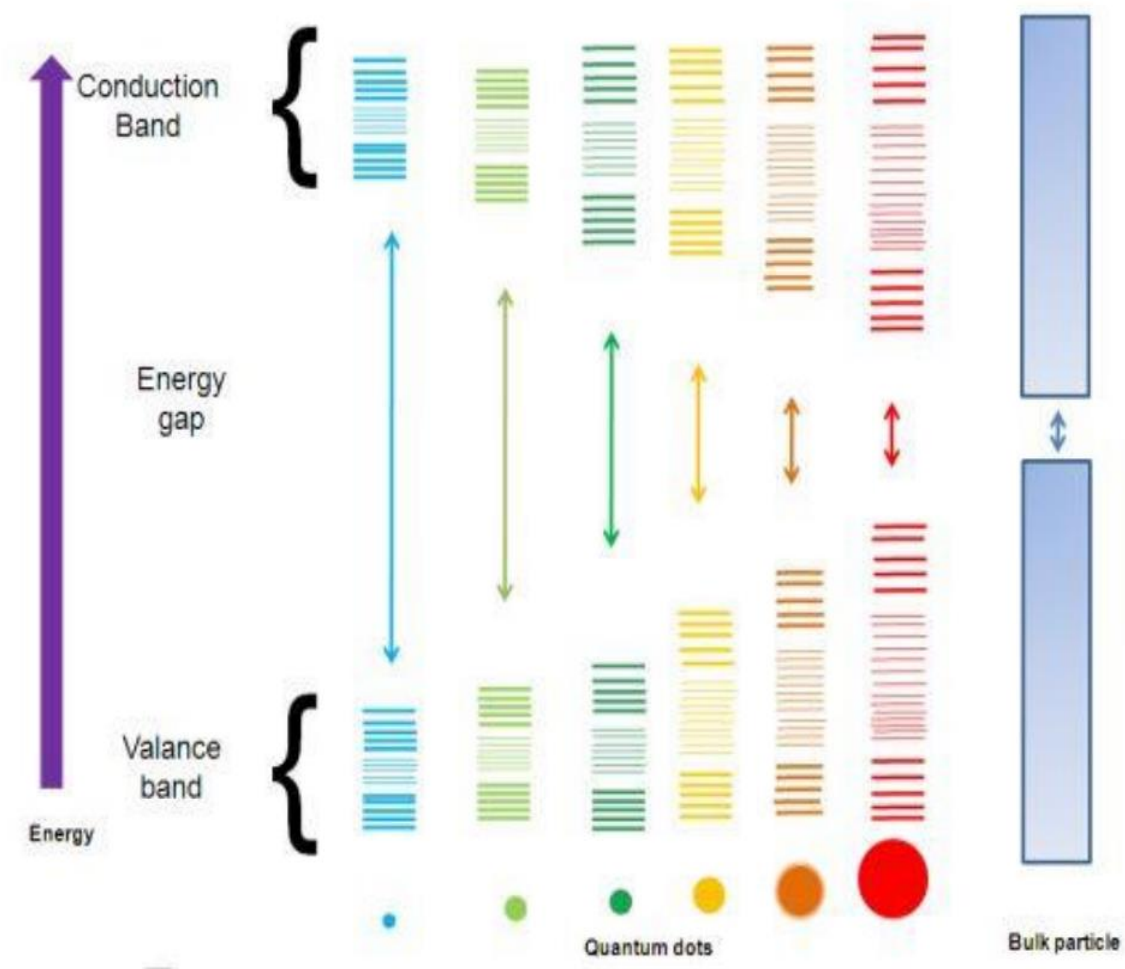

Figure 1.2. Representation of Size-Dependent Optical Properties of Quantum Dots [8]

1.2. Perovskite QDs

Perovskite QDs (PQDs) represent a class of nanoscale semiconductor particles characterized by unique electronic and optical properties. These PQDs have emerged as transformative materials, showing immense promise in diverse technological fields such as LED and solar cells. Their tunable bandgap, high quantum yield, and photostability render them highly desirable for numerous applications.

Perovskite QDs are nanocrystalline structures featuring a perovskite crystal lattice, imparting exceptional electronic and optical characteristics. Unlike conventional semiconductors, PQDs exhibit quantum confinement effects, wherein charge carriers are confined within the nanocrystal, leading to discrete energy levels and a tunable bandgap. This unique property allows precise control over the absorption and emission spectra of PQDs, making them attractive for a wide array of applications [9].

Among the various types of QDs, $CsPb(ClBr)_3$ QDs have emerged as particularly noteworthy.

Comprising cesium (Cs), lead (Pb), chlorine (Cl), and bromine (Br) atoms, these QDs exhibit exceptional optical performance and are suitable for diverse technological applications. $CsPb(ClBr)_3$ QDs hold immense potential owing to their efficiency, stability, and ability to undergo aging processes. The optical performance of $CsPb(ClBr)_3$ QDs is characterized by their emission properties, which are highly dependent on size, composition, and surface passivation. These QDs demonstrate efficient emission across a broad spectrum, making them ideal candidates for vibrant and tunable light emission applications. Moreover, $CsPb(ClBr)_3$ QDs exhibit high photoluminescence quantum yields, indicating their efficiency in converting absorbed photons into emitted light [10].Stability is a crucial aspect of $CsPb(ClBr)_3$ QDs, particularly in practical applications where long-term performance is essential. These QDs demonstrate excellent photostability, retaining their optical properties even under prolonged exposure to light. Furthermore, $CsPb(ClBr)_3$ QDs exhibit robust chemical stability, making them suitable for integrating various devices and systems. Understanding the aging behavior of $CsPb(ClBr)_3$ QDs is essential for optimizing their performance and longevity. Over time, QDs may undergo structural and optical changes due to environmental exposure and interactions with surrounding materials [11]. Investigating the aging mechanisms of $CsPb(ClBr)_3$ QDs provides valuable insights into their degradation pathways and allows for developing strategies to mitigate aging-related effects. $CsPb(ClBr)_3$ QDs represent a promising class of nanomaterials with exceptional optical properties and stability characteristics. This study lays the foundation for a comprehensive understanding of the optical performance, efficiency, stability, and aging behavior of $CsPb(ClBr)_3$ QDs, paving the way for their widespread utilization in various technological applications. Continued advancements in the synthesis, characterization, and application of

$CsPb(ClBr)_3$ QDs hold the potential to drive further innovations and contribute significantly to the development of next-generation optoelectronic devices and systems [12],[13].

1.3 Doped QDs

Doping perovskite QDs with different elements offers a versatile approach to tailor their properties for various applications. It allows for fine-tuning of electronic and optical properties, including bandgap, emission wavelength, and charge carrier mobility, making them suitable for optoelectronic applications [14]. Additionally, doping enhances the stability of perovskite QDs by reducing defect density, preventing phase transitions, and improving resistance to environmental factors such as moisture, heat, and light [15]. Improved charge transport within doped perovskite QDs facilitates enhanced charge separation and reduced recombination losses, which is crucial for high-efficiency solar cells and LEDs [14]. Furthermore, doping can passivate defects within the perovskite lattice, leading to higher photoluminescence quantum yields and improved device performance. It also enables simplified processing and enhanced performance in device fabrication, such as improved film morphology for thin films. Moreover, certain dopants introduce multifunctionality, expanding applications to sensors, catalysis, and spintronics. Controlled emission characteristics, tailored energy levels, and efficient charge injection/extraction further enhance the potential of perovskite QDs for displays, lighting, and quantum information processing. Overall, doping offers a promising avenue to overcome limitations associated with pristine perovskite materials and optimize their properties for diverse technological applications [16].

1.4 QLED

Quantum Dot Light Emitting Diodes (QLEDs) represents a significant advancement in display technology, leveraging the unique optical properties of QDs to produce vibrant, high-quality images. Unlike traditional liquid crystal displays (LCDs), which rely on color filters to generate colors, QLEDs utilize QDs as color converters, offering several advantages, including broader color gamut, higher brightness, and improved energy efficiency [17]. QLED represents a revolutionary advancement in display technology, offering unprecedented levels of color accuracy, brightness, and energy efficiency. QLED displays leverage the unique optical properties of QDs, semiconductor nanoparticles, to produce vibrant images. QLED displays operate on a principle similar to traditional LED displays but with a crucial difference: incorporating a QD layer between the LED

backlight and the display panel. As shown in Figure 1.3 configuration, the LED backlight emits blue light, which passes through a layer of QDs. The QDs absorb this blue light and re-emit it as light of different colors, depending on their size and composition. By precisely controlling the properties of the QDs, manufacturers can achieve a wide range of colors, resulting in vibrant and accurate images on the display panel [18].

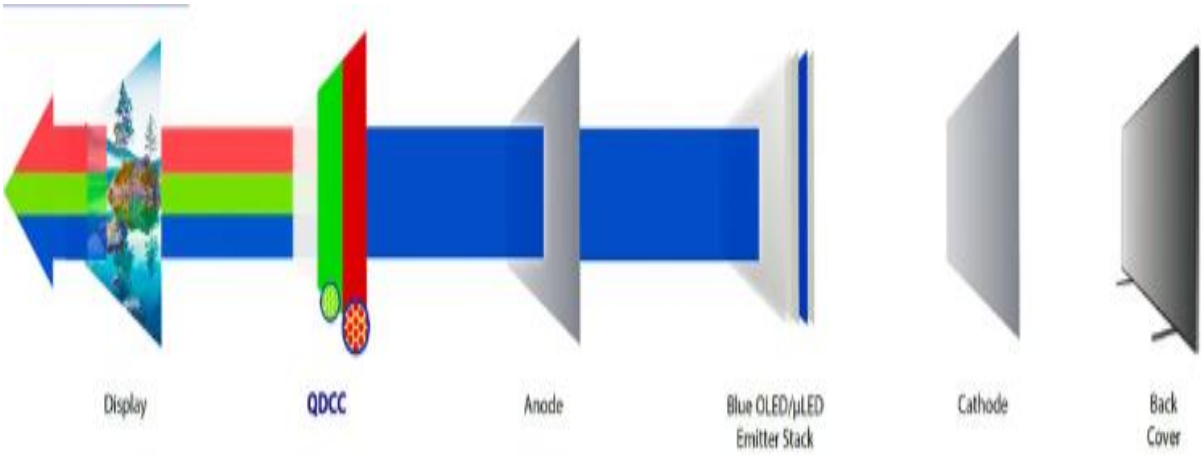

Figure 1.3. The working mechanism of a QLED Display [19]

1.5 Applications of QLEDs

QLEDs have found widespread applications across various sectors, from consumer electronics to healthcare and automotive industries. QLED televisions have gained popularity in consumer electronics for delivering superior picture quality with lifelike colors and enhanced contrast ratios. The wide color gamut of QLED displays ensures accurate color reproduction, making them ideal for viewing high-definition content such as movies, sports, and gaming [20].

Moreover, QLED technology is increasingly being adopted in professional displays and signage applications, where color accuracy and brightness are paramount. QLED displays offer exceptional performance in environments with high ambient light, ensuring visibility and readability even in challenging conditions. Additionally, the energy efficiency of QLEDs translates to lower power consumption and reduced operating costs, making them suitable for large-scale commercial installations. In healthcare, QLED displays are used in medical imaging systems such as radiology monitors and diagnostic displays. The high color accuracy and resolution of QLEDs enable healthcare

professionals to visualize medical images with exceptional clarity and detail, aiding in accurate diagnosis and treatment planning. Furthermore, the stability and duration of QLED technology ensure consistent performance over extended periods, which is critical for reliable medical imaging applications [21].

In automotive applications, QLEDs are employed in dashboard displays, infotainment systems, and heads-up displays (HUDs) to provide drivers with essential information and entertainment content. The high brightness and wide viewing angles of the QLED display ensure visibility and readability in various lighting conditions, enhancing driver safety and convenience. Additionally, the durability and robustness of QLED technology make it suitable for automotive environments characterized by temperature variations and mechanical vibrations [22].

Perovskite Quantum Dot Light Emitting Diodes (PQLEDs) represent a promising advancement in display technology, offering enhanced performance and efficiency compared to traditional QLEDs. PQDs exhibit superior optical properties, including high photoluminescence quantum yield and narrow emission spectra, making them ideal candidates for display applications. PQLEDs have demonstrated exceptional color purity and brightness, enabling the production of displays with vivid and lifelike images [23].

The narrow emission spectra of perovskite QDs ensure precise color control, improving color accuracy and saturation. This makes PQLEDs particularly well-suited for applications requiring accurate color reproduction, such as professional graphics design and content creation. Furthermore, perovskite QDs exhibit excellent stability and longevity, ensuring consistent performance over extended periods. This reliability is essential for applications with critical durability and operational consistency, such as outdoor signage and public displays. Additionally, the solution-processability of perovskite QDs enables cost-effective and scalable manufacturing processes, facilitating the widespread adoption of PQLED technology [24]. In summary, perovskite QLEDs offer significant advantages over traditional QLEDs, including enhanced color purity, brightness, and stability. With their superior optical properties and manufacturing scalability, PQLEDs are poised to drive advancements in display technologies across various sectors, from consumer electronics to automotive and healthcare industries.

1.6. Advantages of QLED Technology

The advantages of QLED technology are manifold, stemming from its unique optical properties and manufacturing advantages. One of the primary advantages of QLED displays is their ability to achieve a wider color gamut compared to traditional displays. QDs offer highly saturated colors and improved color accuracy, allowing for more lifelike and vibrant images. This expanded color palette enhances the viewing experience, particularly for content that demands rich and accurate colors, such as high-definition movies and gaming. Furthermore, QLED displays are renowned for their exceptional brightness levels, surpassing those of conventional displays. QDs exhibit high photoluminescence quantum yields, efficiently converting absorbed photons into emitted light. As a result, QLED displays can achieve higher brightness levels while maintaining energy efficiency. This makes them ideal for use in well-lit environments or outdoor applications where visibility is crucial. In addition to superior color accuracy and brightness, QLED displays offer enhanced energy efficiency compared to traditional display technologies. QDs enable more efficient light conversion, lowering power consumption and operating costs. This energy efficiency benefits consumers by lowering electricity bills and contributes to environmental sustainability by reducing carbon emissions associated with display manufacturing and usage. Another notable advantage of QLED technology is its longevity and reliability [25]. QDs exhibit excellent photostability, meaning they retain their optical properties over prolonged periods, even under continuous exposure to light. This ensures consistent image quality and color accuracy throughout the display's lifespan, minimizing the need for frequent calibration or replacement. Additionally, QLED displays are less susceptible to image burn-in than organic light-emitting diode (OLED) displays, further enhancing their durability and longevity. In conclusion, Quantum Dot Light Emitting Diodes (QLEDs) represent a significant leap forward in display technology, offering unparalleled color accuracy, brightness, energy efficiency, and longevity. By harnessing the unique optical properties of QDs, QLED displays deliver vibrant and lifelike images that captivate audiences across various applications, from home entertainment to professional displays and signage. With continued advancements in manufacturing techniques and materials research, QLED technology is poised to revolutionize the display industry further, paving the way for even more immersive and visually stunning viewing experiences [26].

1.7 QLED Simulations

QLED (Quantum Dot Light Emitting Diode) simulations are computational tools used to model and analyze the behavior of QLED devices. QLEDs are a type of display technology that utilizes QDs to produce light. QDs are semiconductor nanoparticles that emit light when excited by an external energy source, such as an electric current. QLED simulations allow researchers and engineers to study various aspects of QLED devices, including their optical properties, electrical characteristics, and overall performance. Optical simulations of QLEDs focus on modeling the light emission properties of QDs embedded in the device structure. These simulations consider factors such as quantum dot size, composition, and distribution within the device. Optical simulations can predict the emission spectrum, color purity, and brightness of QLEDs under different operating conditions. They also help optimize the design of QLED devices to achieve desired display characteristics, such as wide color gamut and high brightness. Electrical simulations of QLEDs involve modeling the flow of charge carriers (electrons and holes) within the device structure. These simulations analyze the behavior of charge transport layers, injection barriers, and recombination mechanisms in QLEDs. Electrical simulations can predict device performance metrics such as current density, voltage drop, and power efficiency. They also aid in optimizing device architectures and material choices to enhance electrical conductivity and stability. Integrated simulations of optical, electrical, and quantum mechanical aspects enable comprehensive analysis of QLED device performance. These simulations combine optical modeling with charge transport and quantum mechanical calculations to predict overall device efficiency, luminance, and color rendering capabilities. Device performance simulations help guide experimental efforts by providing valuable insights into the underlying physics of QLED operation and identifying strategies for performance optimization [27], [28]. QLED simulations are crucial in designing, optimizing, and understanding QLED devices. Researchers and engineers can accelerate the development of next-generation display technologies with enhanced performance and functionality by leveraging computational tools to simulate and analyze device behavior.

1.8 GPVDM (OghmaNano)

GPVDM (Generalized Photovoltaic Device Model) is a software specifically designed to model and simulate photovoltaic devices, including solar cells and photodetectors. While

its primary focus is photovoltaic devices, GPVDM can simulate other semiconductor devices, including quantum dot-based devices like QLEDs. [29]

Multi-Physics Simulation: GPVDM allows for multi-physics simulations, enabling users to simultaneously model and analyze various physical phenomena. This includes electrical, optical, and thermal effects within the device structure, providing a comprehensive understanding of device behavior. Quantum Dot Modeling: GPVDM includes models and algorithms for accurately simulating the behavior of QDs within the device. This includes modeling of quantum confinement effects, energy levels, and carrier dynamics specific to quantum dot materials. Material Properties: The software consists of databases of material properties relevant to semiconductor devices, allowing users to specify the properties of quantum dot materials and other constituent layers within the device structure. Device Architecture: GPVDM supports the modeling of complex device architectures commonly found in QLEDs and other semiconductor devices. Users can define the layer structure, interfaces, doping profiles, and other parameters to represent the device under study accurately. Optical Properties: GPVDM incorporates optical modeling capabilities to simulate light absorption, emission, and propagation within the device. This allows users to predict the optical characteristics of QLEDs, including emission spectra, color rendering, and external quantum efficiency. Performance Analysis: The software provides tools for analyzing the performance of QLEDs and other semiconductor devices. This includes calculating key metrics such as current voltage characteristics, luminance, power conversion efficiency, and spectral response. User Interface: GPVDM typically features a user-friendly interface that allows users to define device parameters, set up simulations, visualize results, and analyze data. This makes it accessible to researchers and engineers with varying levels of simulation expertise. GPVDM is a powerful tool for modeling and simulating QD-based devices such as QLEDs. By accurately capturing the underlying physics and material properties, GPVDM enables researchers to explore device performance, optimize device designs, and guide experimental efforts in developing next-generation optoelectronic devices [30].

1.9 Literature Review

PQDs have garnered significant attention due to their unique optical properties, including tunable wavelength, narrow emission spectra, and high photoluminescence quantum efficiency (PLQY). Hung-Chia Wang and Zhen Bao introduce new PQD variants and propose strategies to improve their stability. Future applications of PQDs in light-emitting

diodes are also discussed, highlighting their potential in advancing optoelectronic technology [31].

Li, Qing, et al. successfully show that UV emission in QLEDs is attributed to the recombination of electrons and holes occupying quantum-confined levels. They found that MgO is an appropriate shell material for core-shell structures due to its excellent confinement effect, as its energy gap (Eg) is nearly twice that of ZnO, contributing to improved Near Band Edge (NBE) efficacy. Furthermore, they discovered that the thickness of the Hole Injection Layer (HIL) and Hole Transport Layer (HTL) significantly influences the UV emission properties of the device. They concluded that all solution-processed ZnO-MgO QD materials hold promise for UV QLED applications. However, they note the need to address visible light emission from other materials, such as PEDOT: PSS, in further research to realize the full potential of UV QLED technology [32]. Lee, Taesoo, et al. present a breakthrough in QLEDs, addressing their historical limitations and significantly advancing their potential for next-generation displays and lighting sources. By focusing on two key aspects, tailored quantum dot interfaces and optimized device architecture, they achieve bright and stable QLEDs on a silicon substrate, expanding their application possibilities beyond current limitations. Firstly, the researchers engineered a specialized interface for the QDs, maximizing their quantum yield and reducing nonradiative Auger decay, which is crucial at high current densities. Secondly, they employ and optimize a top-emission device architecture capable of withstanding high temperatures, enhancing light outcoupling efficiency [33]. There are no direct applications of QLEDs using gpvdm simulation, but many OLED applications exist. Gamal, Shaimaa, Ihab E. Talkhan, and Tawfik Ismail focused on the OLED, a significant advancement in LED technology widely utilized in various applications today. Specifically, the Alq_3 OLED structure, incorporating high-efficiency optical materials such as TPD and Alq_3, is examined. These organic light-emitting layers are situated between electrical contacts, with the anode typically made of indium tin oxide (ITO) and aluminum-lithium (Al/Li) cathode. The article reports on the modeling and simulation of the Alq_3 OLED, both before and after incorporating quantum well (QW) structures, utilizing the GPVDM simulation. A reverse voltage of -2.24 V is applied to the OLED, and various metrics such as light output current density variance curves, light flux, and current are analyzed [34].

Another study, Atik, İpek, et al., focuses on the structural characteristics of OLEDs, explaining the band model and functional properties. A three-layer OLED design is proposed, incorporating high-efficiency optical materials such as IRPPY, BCP, and Alq_3. General-purpose Photovoltaic Device Model (gpvdm) simulation software is utilized for analysis, determining bandwidth values for each layer and selecting Indium Tin Oxide (ITO) for the anode and Silver (Ag) for the cathode. The designed OLED is subjected to electrical circuitry with voltage ranging from -0.2V to 2.5V, resulting in light output power variance curves. Energy level variance curves of the lowest unoccupied molecular orbital (LUMO) and highest occupied molecular orbital (HOMO) are obtained using Maxwell-Boltzmann statistical features. Photon density emitted by the optical materials and energy-location variance data are also analyzed[35].

2. MATERIALS AND METHODS

2.1 EXPERIMENTAL SECTION

Preperation of Cs-least; 0.2035 gr Cs_2CO_3 was mixed with 10 ml ODE(Octadecane) and 0.625 ml of oleylamine in a three-neck flask, and the solution was dried under vacuum for 1 hour at 120 °C. Then, the atmosphere of the solution changed to the nitrogen at 130 °C to dissolve the Cs_2CO_3. Lastly, the temperature decreased to 100 °C for injection. Synthesis of $CsPb(ClBr)_3$ QDs 1.5 ml Oleylamine, 1.5 ml Oleic acid, 15 ml of octadecane, 0.54 mmol $PbCl_2$ and 0.54 mmol of $PbBr_2$ were mixed and heated at 120 °C for one hour under the vacuum. Then, the heat was increased to 170 °C, and the solution got under the nitrogen gas. 1 ml of Cs-oleate solution was quickly added, and 10 seconds were waited. Lastly, the solution was cooled to room temperature in an ice bath.

Synthesis of $CsPB(ClBr)_3$:Zn (1:1, 0.8:0.2, 0.6:0.4, 0.4:0.6 ratios) doped QDs.

0.75 ml OA, 0.75 ml OLA, 0.75 ml ODE, 0.2 gr $PbBr_2$ and different ratios of $PbCl_2$ and $ZnCl_2$ (due to molar ratio of doped Zn) were added in a three-neck 100 ml flask and stirred under the vacuum at 120 °C for an hour. Then, the temperature was raised to 196 °C, and 0.5 ml Cs-oleate was added to the solvent very quickly. After 10 seconds, the solution is put into the ice bath to cool down to room temperature.

Figure 1.4 shows the synthesized QDs. After the synthesis, the QDs were placed in tubes under a nitrogen gas atmosphere.

When exposed to ultraviolet light, the QDs exhibited photoluminescence, emitting a yellow-colored light depending on their size and composition.

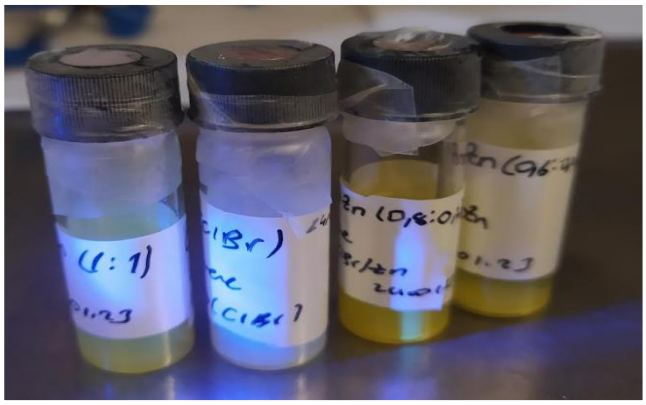

Figure 1.4. Images of the synthesized qdots

2.2 SIMULATION OF QLED

Their device structure significantly influences the performance and efficiency of QLEDs. Achieving high-performance displays requires a carefully designed device structure that optimizes charge transport, light emission, and overall functionality. This involves selecting and arranging materials to facilitate efficient charge injection, transport, and recombination, impacting crucial aspects such as color purity, luminance, and operational stability. Three different device structures were designed in a specific case study, each incorporating specific layers to enhance performance. ITO contact is a transparent and conductive electrode; the ITO layer enables efficient charge injection into the QLED structure. PEDOT: PSS represents the hole transfer layer, facilitating the transport of positive charges (holes) from the anode to the active layer. $CsPb(ClBr)_3$ represents the active layer emitting light when excited by electrons and holes, resulting in the desired color output. Zinc oxide (ZnO) acts as an electron transfer layer, facilitating the transport of negative charges (electrons) from the cathode to the active layer. Lithium flüoride (LiF) is a hole injection layer. This layer receives holes from the anode and injects them deeper into the device. As a cathode, the Al layer allows efficient charge extraction from the QLED structure [36].

Figure 2.1 shows the graphical representation of the structure of a QLED device in GPVDM. Each layer is represented with a different color.

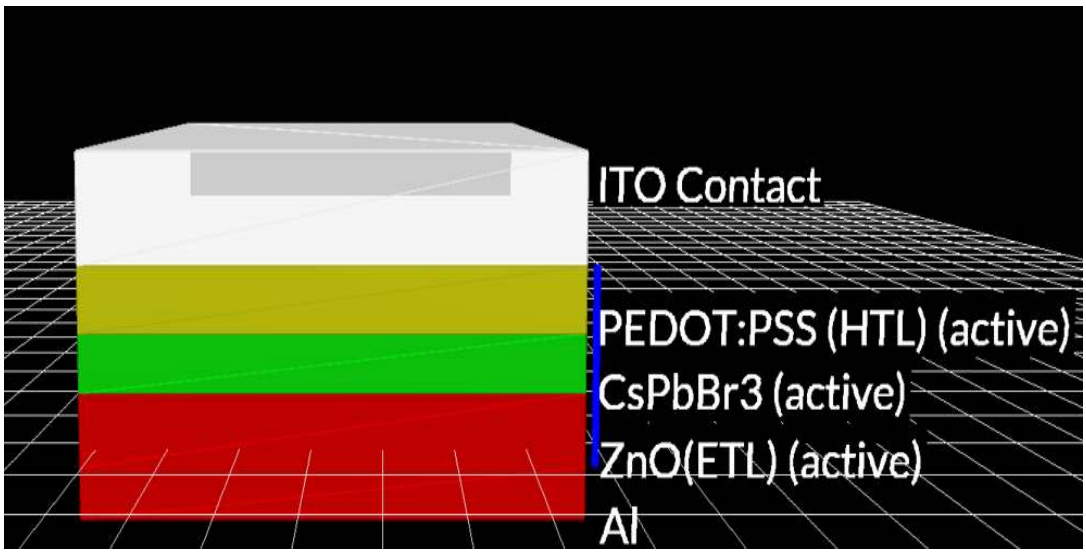

Figure 0.1. The structure of QLED device

Figure 2.2 shows how to open the materials database in the gpvdm program. There is a section called ‘databases’ on the top right side. Clicking there shows the options in this section. The materials database is the one needed.

Figure 2.2 Table of adding new materials

Figure 2.3 shows the screen after clicking the materials database. Click 'add material' at the top right of the window to bring up a dialogue box asking for a new name for the material.

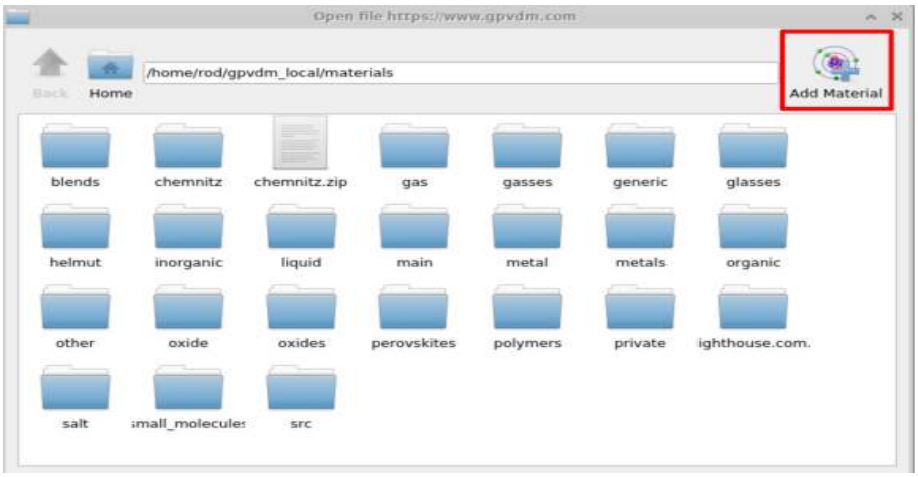

Figure 2.3. Materials Database Box

Figure 2.4 shows the dialogue box for giving the new material a name. Any name can be given, but using the correct description is essential.

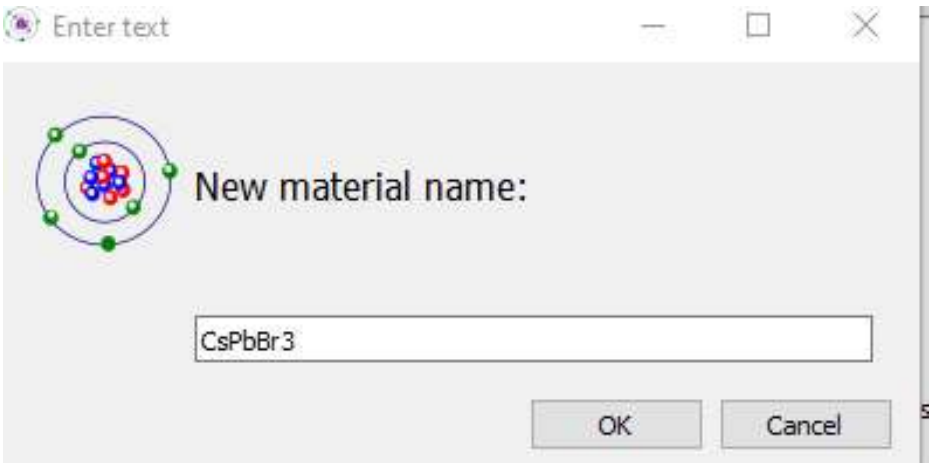

Figure 2.4. Table of typing the name of new materials

Figure 2.5 shows the dialogue box for adding the new material's data. The material's absorption, refractive index, and electrical and thermal parameters are needed. In this study, CsPbBr3 QD was added to the library, and those parameters were provided by literature research.

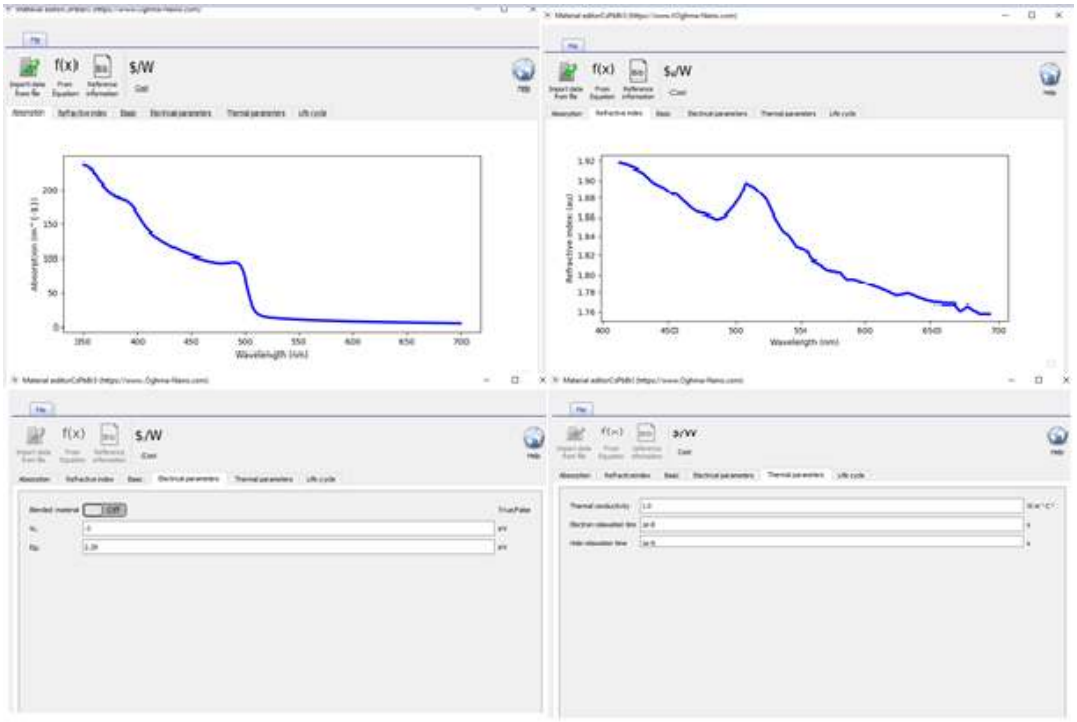

Figure 2.5 Table of adding materials database

In GPVDM, device structures are represented as a series of layers. These layers can be edited using the layer editor, accessible from the main simulation window under the device structure tab. Within the layer editor window, there is a table that outlines the structure of the device. Each row in the table corresponds to a layer, and the "thickness" column indicates the thickness of each layer, as shown in Figure 2.6. Layer type specifies to the simulation how the layer is treated when performing a simulation. There are three types of layers. The active layer is electrically active, and the drift-diffusion solver will solve the electrical equations in this layer type. You can have as many active layers as you like, but they must be contiguous. The contact layer tells the model that a layer is a contact and a voltage should be applied. The other layer is any layer that is not in contact or active [37].

Layer name	Thicknes (m)	Optical material	Layer type
ITO Contact	1.5e-07	... oxides/ito	other
PEDOT:PSS	4e-08	... polymers/pedotpss	active layer
CsPbBr	3e-08	... CsPbBr3	active layer
ZnO	5e-10	... chemnitz/ZnO	active layer
LiF	5e-08	... metal/al	other
Al	5e-08	... metal/al	other

Figure 0.6. The layer structure of the device with the LiF layer

In Figure 2.6, the incorporation of a HIL is highlighted, with LiF serving as the chosen material for this critical component. Figure 2.6 provides a closer look at the specific role of LiF as the hole injection layer in the QLED device structure. LiF is a barrier layer that helps to align the energy levels between the anode and the hole transport layer, reducing energy barriers for hole injection and enhancing charge injection efficiency. Additionally,

LiF assists in smoothing the energy landscape at the anode/HTL interface, minimizing charge trapping and improving charge transport properties within the device [38].

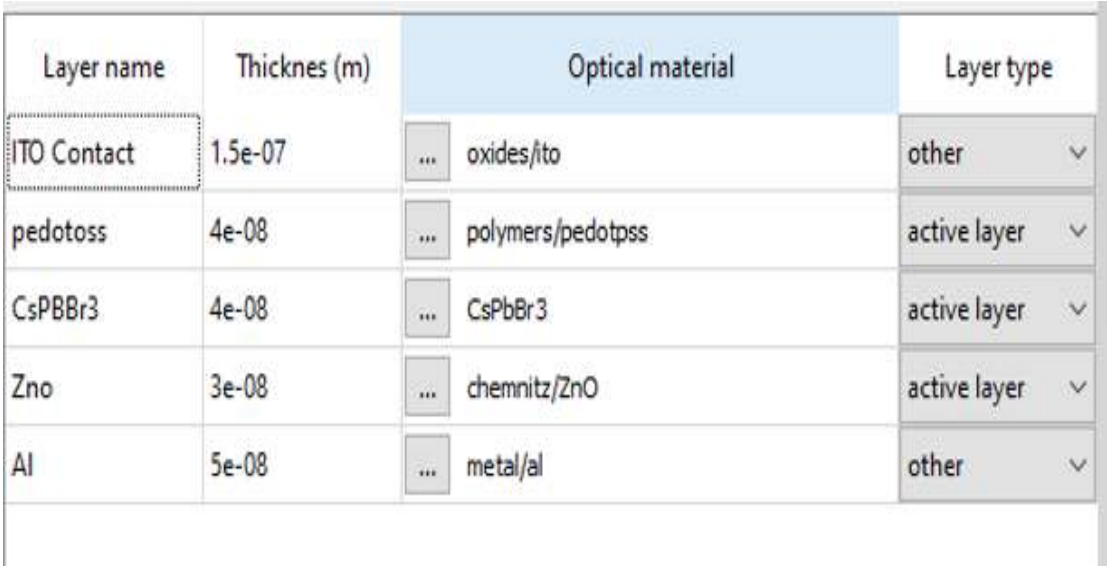

Layer name	Thicknes (m)	Optical material	Layer type
ITO Contact	1.5e-07	... oxides/ito	other
pedotoss	4e-08	... polymers/pedotpss	active layer
CsPBBr3	4e-08	... CsPbBr3	active layer
Zno	3e-08	... chemnitz/ZnO	active layer
Al	5e-08	... metal/al	other

Figure 0.7. The layer structure of the device with 40 nm thick $CsPb(ClBr)_3$ active layer without LiF layer [xi]

Figure 2.7 shows the structure of the device with a thicker, which is 80 nm $CsPb(ClBr)_3$ active layer. The layered structure of QLED devices plays a pivotal role in facilitating efficient charge injection, transport, and light emission processes, ultimately influencing device performance and functionality. Understanding the composition and arrangement of these layers is essential for optimizing device design and enhancing device efficiency [39].

3. RESULTS and DISCUSSION

3.1 Optical Properties of $CsPb(ClBr)_3$ and Zn doped $CsPB(ClBr)_3$ QDs

In this thesis, the optical properties of $CsPb(ClBr)_3$ QDs investigated through Zn doping at varying ratios (0.4, 0.6, 0.8, 1). The thesis includes a detailed daily PL and UV-Vis absorbance spectra analysis for each doping ratio. PL spectra reveal the temporal evolution of optical properties for different Zn-doped $CsPb(ClBr)_3$ QDs. Simultaneously, UV-Vis absorbance plots provide information on the stability of absorption properties at each Zn doping ratio, highlighting changes or trends over time. A comparison of these data at various Zn doping ratios allows for a broad assessment of the effect of Zn concentration on both photoluminescence and absorption properties. These findings include valuable information regarding the daily degradation behavior and overall stability of Zn-doped $CsPb(ClBr)_3$ QD [40].

In this study to compare undoped and doped quantum dots 0,6 ratio Zn doped quantum dot were used, it was found that quantum dots doped at a ratio of 0.6 yielded better results.

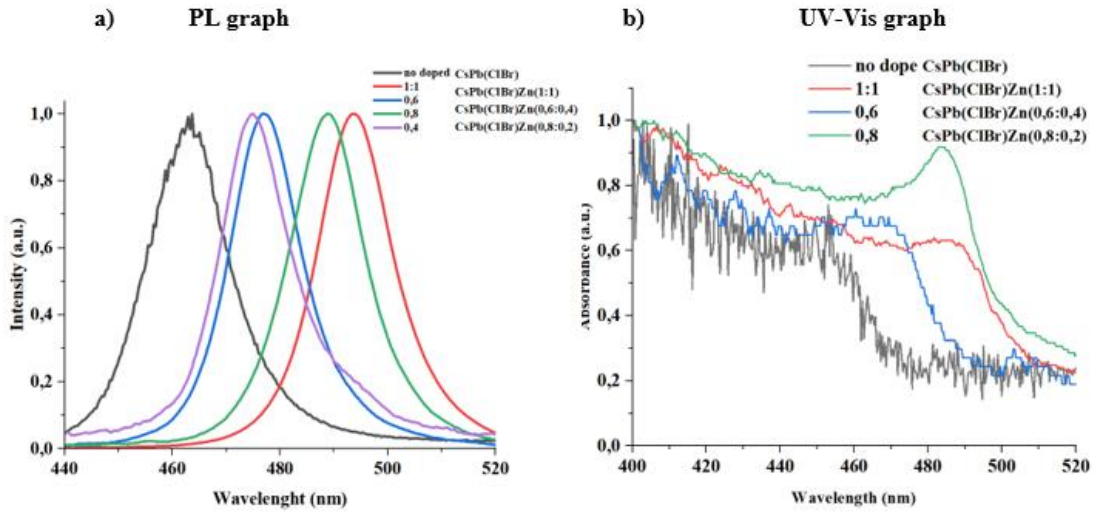

Figure 3.1 a) PL graph of each $CsPb(ClBr)_3$ QDs (1doped, 0.8 Zn doped. 0.6 Zn doped, 0.4 Zn doped and no doped QD) b) UV-Vis spectra of all samples.

In Figure 3.1, the intensity (PL) graph of the five QDs reveals a distinctive trend as the doping ratio increases. Increasing the molarity of doped Zn slides the PL of $CsPb(ClBr)_3$ QDs to 460 nm to 505 nm. The wavelength shift provides a smooth color transition to the QDs. The 0.4 Zn-doped QD, 0.6-doped QDs, and 0.8-doped QD show a gradual rightward shift on the graph, with the peak intensity occurring at successively longer

wavelengths. This shift in peak wavelength suggests that the introduction of doping alters the electronic and optical properties of the QDs. Specifically, the increase in doping ratio appears to lead to a redshift in the emission spectrum. This phenomenon can be attributed to changes in the quantum dot's band structure and energy levels due to the incorporation of dopant atoms. Notably, the first exciton absorption features, especially in Zn-doped samples, are discernible, affirming a higher confinement degree in Zn-doped compared to undoped samples. The sharp 1S absorption features exhibit a tunable range from 454 nm to 485 nm. The red-shift in excitonic bandgap with increasing Zn ratio is attributed to lattice size contraction resulting from the replacement of Pb+2 ions with Zn+2 ions. Correspondingly, the sharp PL spectra display a redshift from 470 nm to 488 nm with increasing Zn content. Significantly the FWHM of undoped samples is notably more significant (25 nm) than that of Zn-doped samples (18 nm), indicating a higher order of size monodispersity in the latter. The stoke shift of Zn-doped samples is approximately four times smaller than that of undoped samples, attributed to morphological differences between the doped and undoped samples [41].

In Figure 3.2, the absorbance spectra of 0.4 Zn-doped $CsPb(Cl/Br)_3$ QDs exhibit a consistent peak around 480 nm across the observed 4-day period. Similar to graph 'a', the 0.6 Zn-doped $CsPb(Cl/Br)_3$ QDs display a stable peak around 490 nm throughout the 4-day duration. The absorbance spectra for 0.8 Zn-doped $CsPb(Cl/Br)_3$ QDs consistently show a peak around 497 nm over the three days. The 1:1 Zn-doped $CsPb(Cl/Br)_3$ QDs exhibit a stable absorbance peak around 500 nm throughout the 5-day observation. It is noteworthy in the Uv-Vis graphs that the absorbance levels decrease day by day. This trend indicates a gradual decrease in the concentration or optical activity of QDs. Also, the decreasing absorbance levels over time suggest a reduction in the population of active QDs or changes in their optical properties. The gradual decrease in absorbance levels over time in all plots implies a time-dependent reduction in the concentration or optical efficiency of Zn-doped $CsPb(Cl/Br)_3$ QDs. Changes in absorbance levels between different doping ratios indicate that the extent of Zn doping affects the overall absorbance intensity and optical properties. In conclusion, these graphs collectively underscore the dynamic nature of Zn-doped $CsPb(Cl/Br)_3$ QDs' UV-Vis absorbance, emphasizing the importance of careful consideration of doping ratios and temporal effects in applications requiring stable optical performance [42].

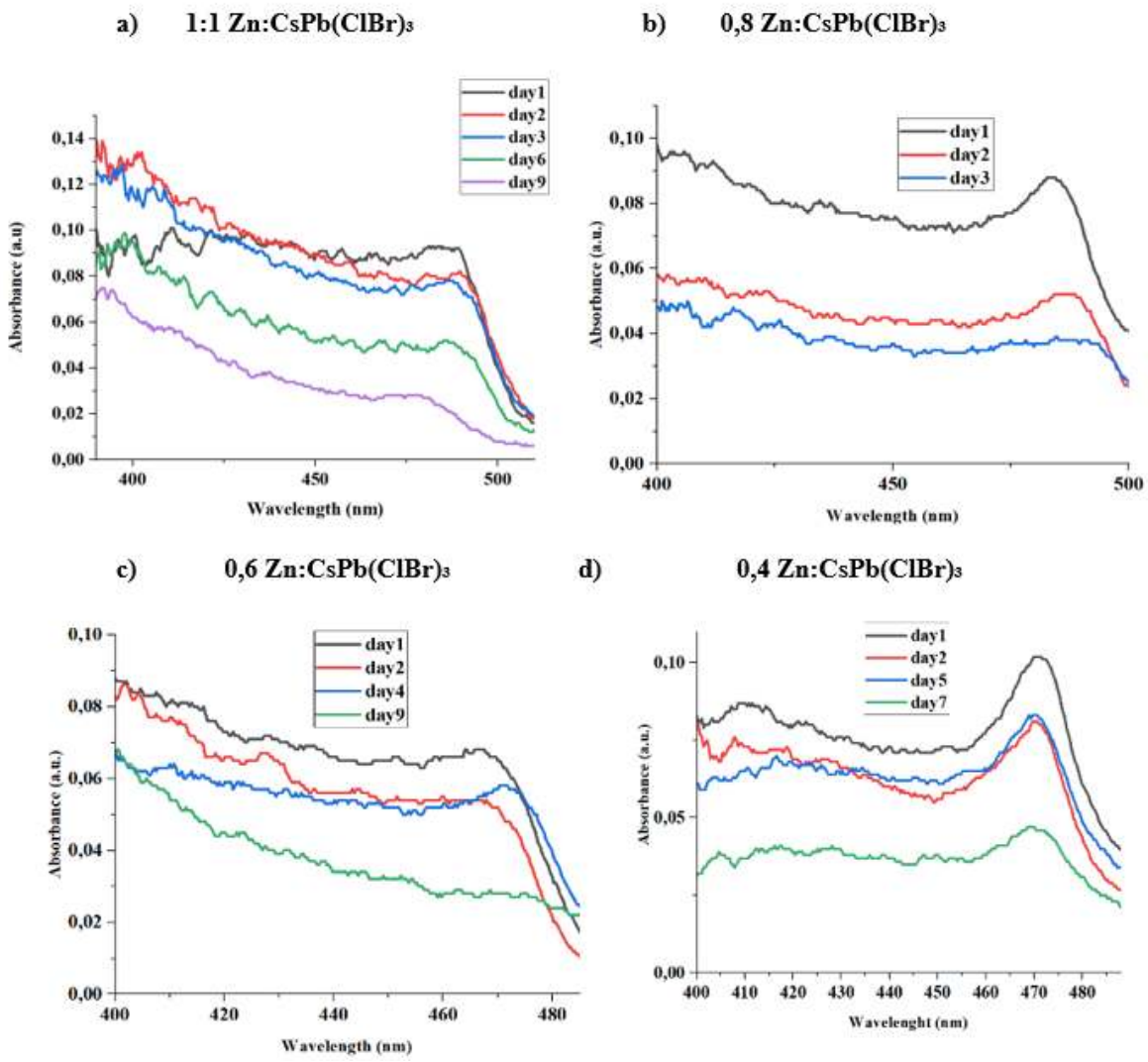

Figure 3.2. The presented set of graphs (labeled a, b, c, and d) provides a comprehensive insight into the UV-Vis absorbance behavior of Zn-doped $CsPb(ClBr)_3$ QDs (QDs) at varying Zn doping ratios over alternate days

Over seven days, a comparative analysis of normalized photoluminescence (PL) spectra for both doped and undoped samples to investigate the impact of Zn doping on the stability of $CsPb(Cl/Br)_3$ QDs. Figure 3.3 shows the PL spectra for doped and undoped samples. The corresponding PL peak positions and FWHM values are presented in Figure 3.6. Interestingly, the PL spectra of the undoped sample exhibit erratic behavior, with peak positions and FWHM values fluctuating between 469-483 nm and 24-14 nm. This suggests an increase in the influence of surface trap states over time in undoped samples. In contrast, the PL spectra of the Zn-doped sample show minimal changes over the specified period. The peak position and FWHM values remain consistent for at least seven

days, unlike the undoped sample. These findings affirm that the introduction of Zn ions significantly enhances the time-dependent PL stability of $CsPb(ClBr)_3$ QDs as illustrated in Figure 3.3[46].

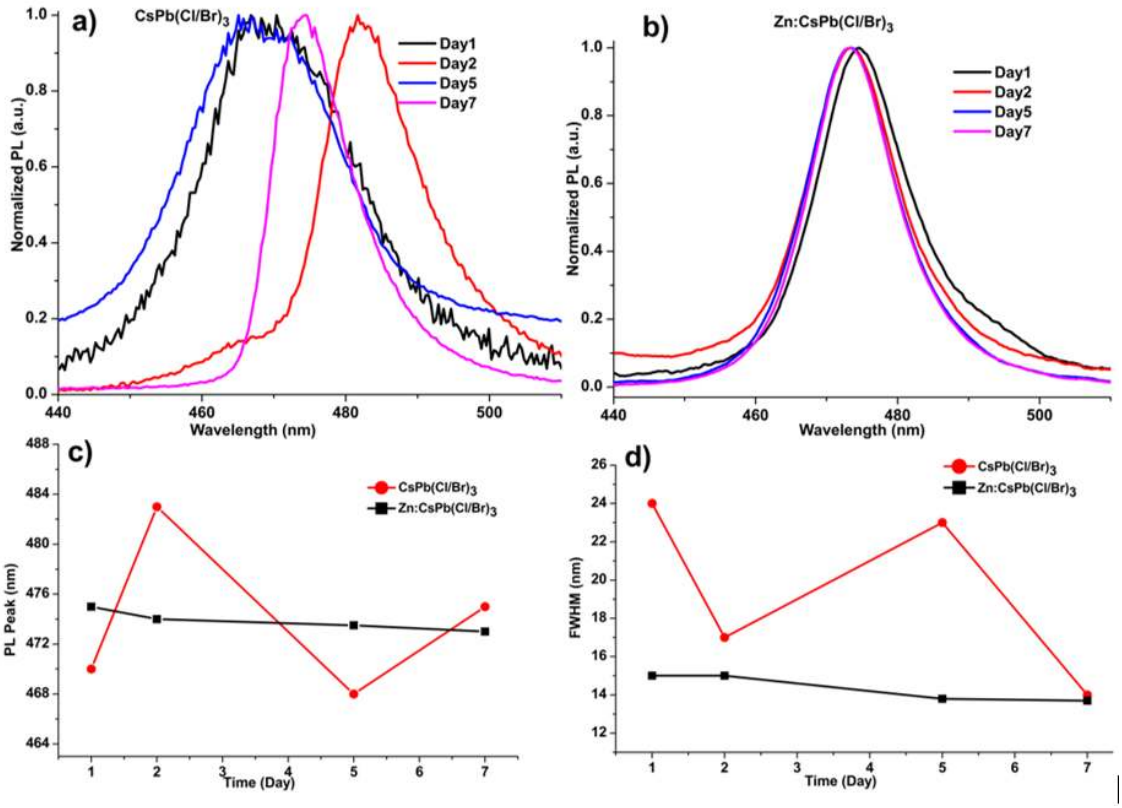

Figure 3.3. Time evolutions of the normalized PL spectra of undoped (a) and Zn doped (b) $CsPb(ClBr)_3$ QDs and the corresponding time-dependent PL peak (c) and FWHM (d) values.

In Figure 3.4, the laser power-dependent photoluminescence (PL) spectra show different behaviors between the undoped and Zn-doped quantum dots (QDs). The PL peak position and shape do not change with varying excitation power for the Zn-doped sample. However, the PL peak position in the undoped sample undergoes a slight red shift at high excitation powers, indicating that sub-bandgap recombinations play a more significant role in the undoped material. The PL intensity increases linearly with excitation power for both samples, suggesting the emission is primarily due to radiative recombination of excitons, as observed in the UV-Vis spectra. The linear trend also indicates the samples have a high density of states and low surface traps. However, the slope is lower for the Zn-doped sample (~1.2) than the undoped sample (~1.7),

indicating reduced non-radiative recombination in the Zn-doped QDs. Doping $CsPb(ClBr)_3$ QDs with Zn significantly enhances the PL properties of the material [44].

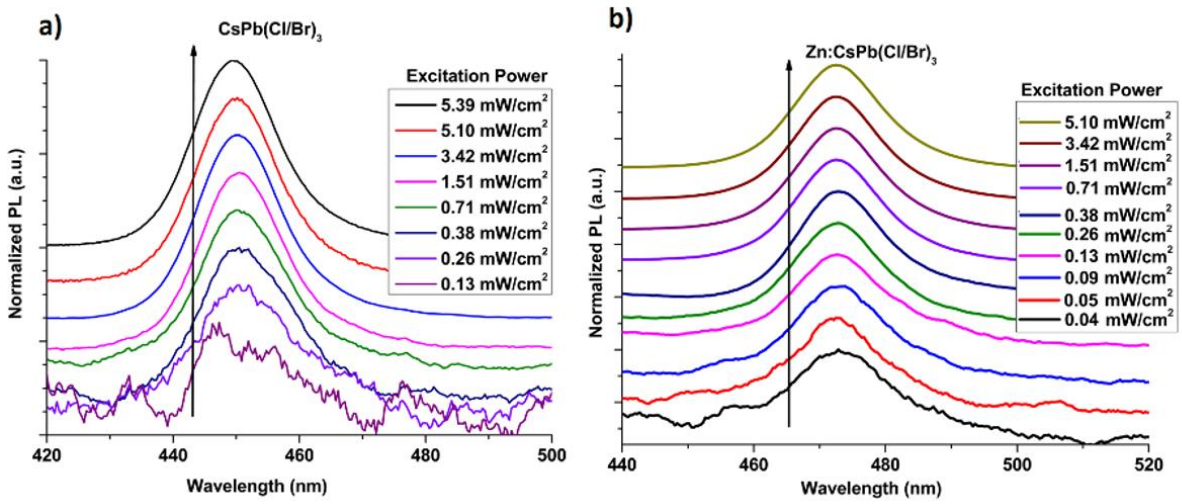

Figure 3.4. Representation of power-dependent graph of no doped $CsPb(ClBr)_3$

Experimental results reveal exciting trends in the photoluminescence of $CsPb(ClBr)_3$ QDs by comparing undoped and 0.6% zinc doped at various temperatures. The common observation of a decrease in peak intensity as temperature increases is consistent with expectations and reflects typical changes in exciton recombination rates due to increasing thermal energy. The more intriguing finding is the wavelength shift observed only in doped QDs. A blue shift is observed with increasing temperature. One possibility that may be the cause is the effect of quantum confinement effects, where doping-induced changes in the size or structure of the quantum dot affect its optical properties. Zinc could introduce additional energy levels or change the band structure, potentially contributing to the observed blue shift. In temperature-dependent processes, doped QDs may interact differently with electronic transitions than undoped ones, leading to different behavior. The fact that undoped QDs do not exhibit a significant wavelength shift implies that zinc doping is a crucial factor. The blue shift observed in doped QDs indicates complex interactions between temperature, doping, and quantum dot structure. So, in Figure 3.5, zinc doping plays a crucial role in the temperature-dependent photoluminescence behavior of $CsPb(ClBr)_3$ QDs, especially causing a blue shift in the emission peak [45].

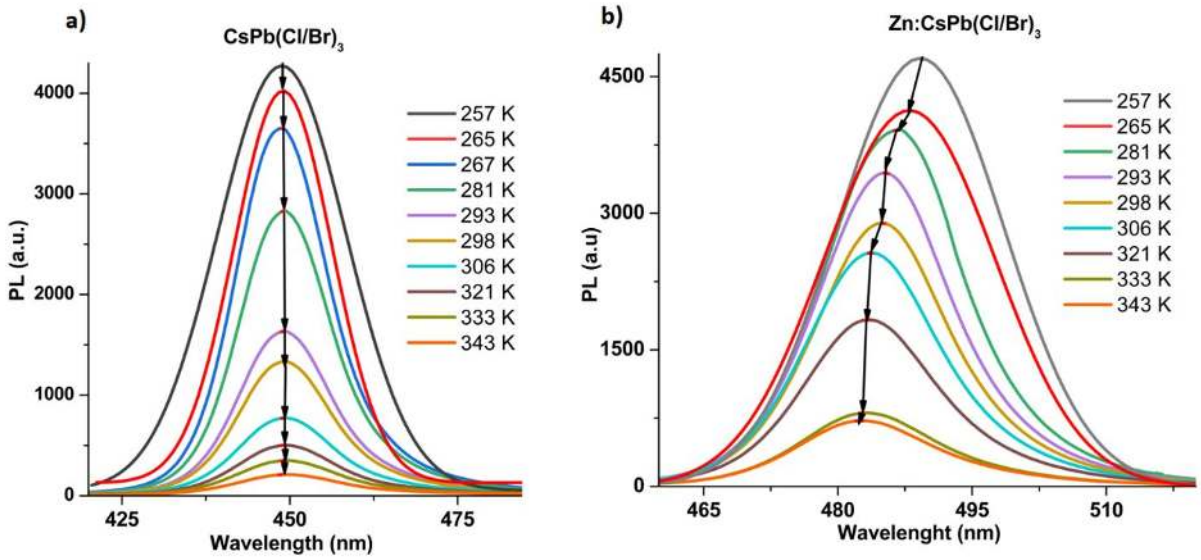

Figure 3.5. a) Temperature-dependent graph of 0, 6 Zn doped CsPb(ClB)r$_3$ b) Temperature-dependent graph of no doped CsPb(ClBr)$_3$

Light exposure can degrade the properties of quantum dots, so careful control of light conditions is necessary to understand their photoluminescence performance. The effects of UV light exposure (370 nm, 9 W) were comparatively investigated for the Zn-doped and undoped QD samples, as shown in Figure 3.6. The PL intensity of both samples decreased as the UV exposure time increased. However, the PL intensity decreased at a higher rate in the undoped CsPb(Cl/Br)3 QDs compared to the Zn-doped QDs. Additionally, while the PL peak position remained constant for the undoped QDs, the Zn-doped sample underwent a blue shift. These results indicate that doping CsPb(ClBr)$_3$ QDs with Zn significantly enhances their photostability and resistance to photoactivation and surface trap effects under UV light exposure, compared to the undoped material.

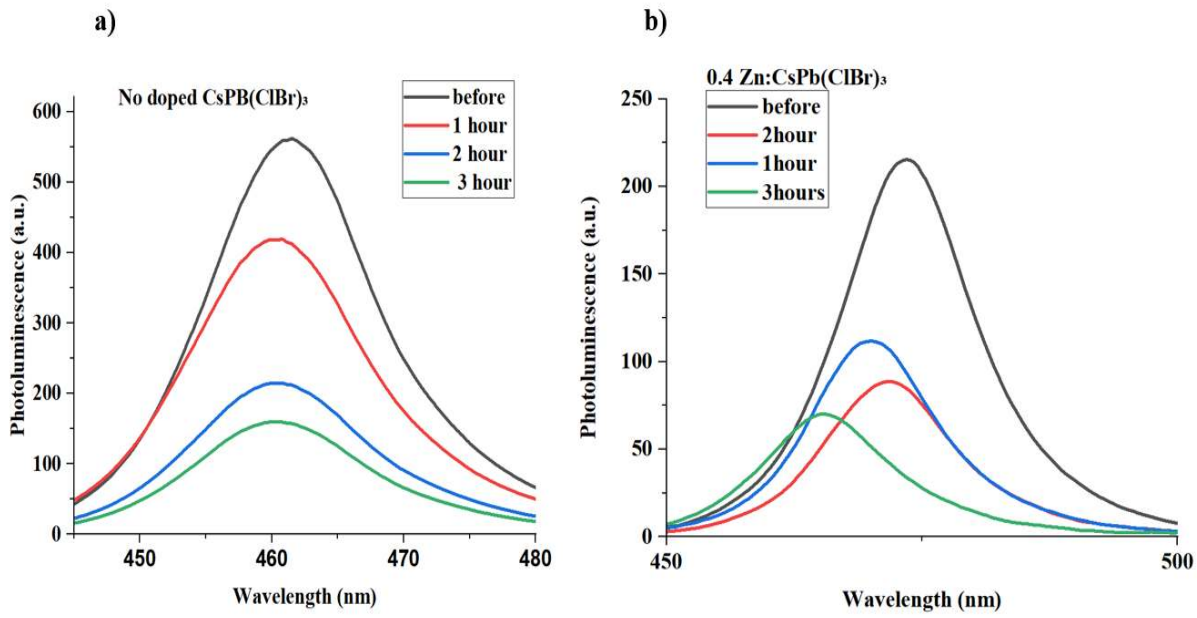

Figure 3.6. a) Aging graph of no doped $CsPb(ClBr)_3$ under UV-light b) Aging graph of 0.4 $CsPbClBr_3$ under UV-light

In some types of quantum dots (QDs), the emission peak has been observed to depend on the concentration of the solution, which is typically attributed to photon reabsorption. In this study,undoped $CsPb(ClBr)_3$ QDs exhibit a blue shift in the photoluminescence (PL) spectra as the solution concentration increases, as shown in Figure 3.7. As the QD solution concentration increases, the PL peak shifts from right to left and stabilizes while the PL intensity increases. This behavior is the opposite of what is expected from the photon reabsorption mechanism, which typically causes a red shift in the PL peak and a decrease in PL intensity. To the researchers' knowledge, this type of behavior has not been previously observed in QDs. They suggest that an anti-Stokes PL mechanism may be responsible for the blue shift in the PL spectra. The potential reasons for this anti-Stokes shift could be two-fold: 1) at high QD concentrations, the distance between QDs decreases, leading to enhanced quantum confinement effects through inter-QD interactions, and 2) at high concentrations, the surface trap density increases, which may influence the electronic structure of the QDs. Despite these proposed explanations, the researchers acknowledge that more research is needed to fully elucidate the precise mechanism behind the concentration-dependent blue shift in the PL spectra of the undoped $CsPb(ClBr)_3$ QDs [46].

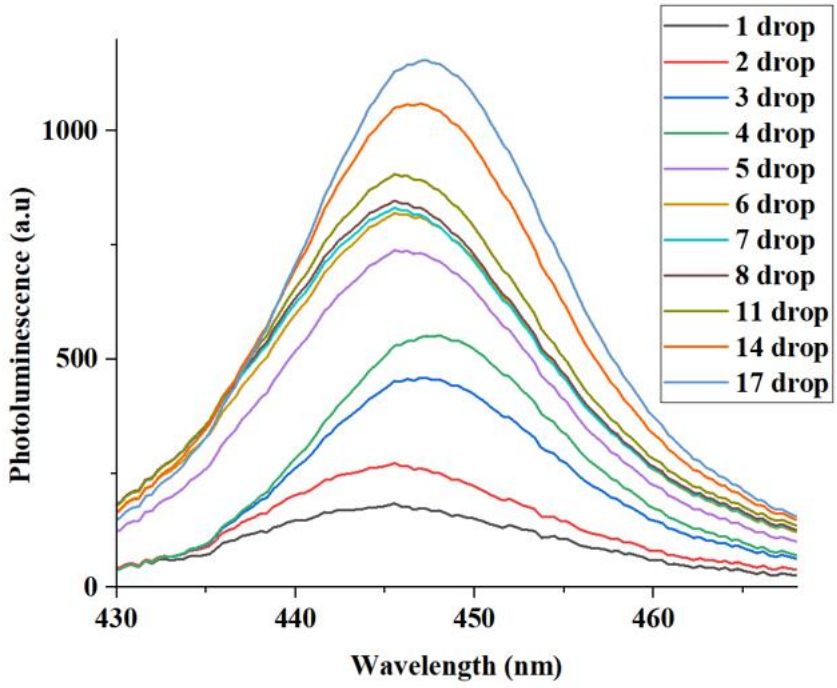

Figure 3.7.) Concentration dependent PL spectra of $CsPb(ClBr)_3$

3.2 $CsPbBr_3$ GPVDM Simulations

Figure 3.8 depicts the current-voltage characteristics of three distinct QLED device structures: those with a LiF layer, those without a LiF layer, and those featuring an 80 nm thick $CsPbBr_3$ active layer. The comparison illustrates the influence of different structural parameters on device performance. Upon examination of the current output curves, it becomes evident that the presence or absence of the LiF layer and the thickness of the $CsPbBr_3$ active layer significantly impact the device's electrical behavior. Notably, the current voltage graph highlights distinct trends among the different structures. The plot reveals that devices with and without the LiF layer exhibit comparable current levels, indicating that the presence of the LiF layer does not drastically affect the device's current flow. However, a notable deviation occurs with the device featuring an 80 nm thick $CsPbBr_3$ active layer. In contrast to the other structures, the device with the thicker $CsPbBr_3$ active layer demonstrates reduced current flow. This observation suggests that increasing the thickness of the active layer beyond a certain threshold may hinder the efficient flow of current through the device. Such behavior could arise due to increased charge carrier recombination or altered charge transport mechanisms within the thicker

active layer. The device with a LiF layer gives the best output due to the work function matching between the ZnO and HIL layers [47].

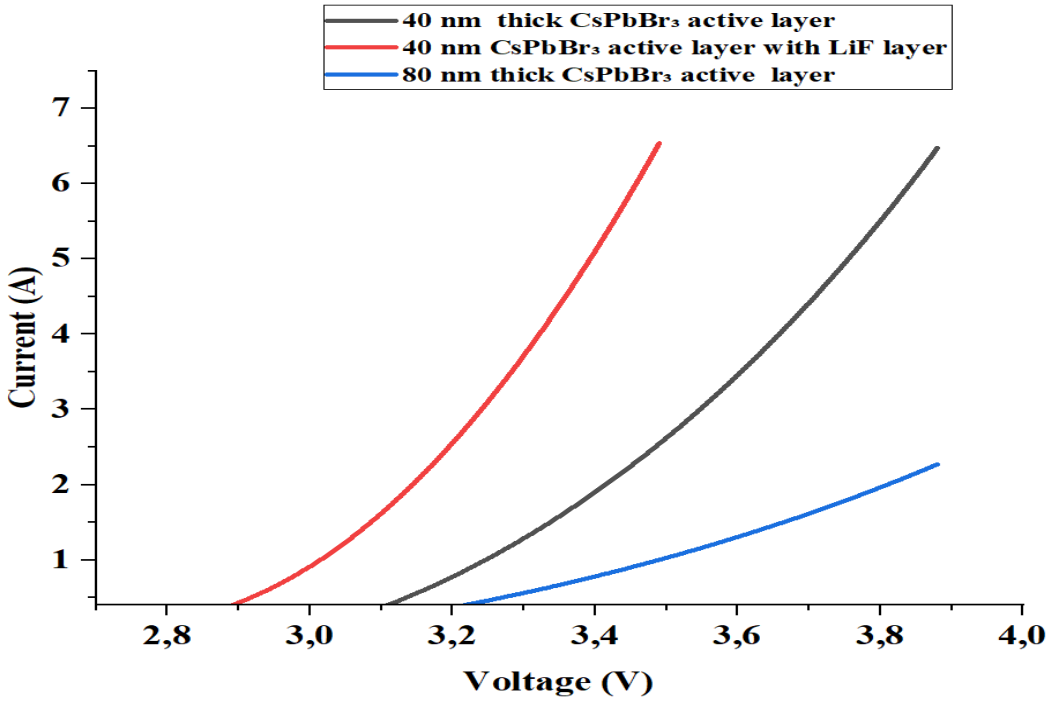

Figure 3.8. Current graph of Qled devices' structure with LiF layer, without LiF layer and 80 nm thick $CsPbBr_3$ active layer

Figure 3.9 presents the current-voltage characteristics of QLED devices featuring varying thicknesses of the $CsPbBr_3$ active layer, specifically 30 nm, 40 nm, 50 nm, and 80 nm and the device with the HIL layer.Due to the analysis of the current output curves, it becomes evident that the thickness of the $CsPbBr_3$ active layer plays a crucial role in determining the device's electrical behavior The plot showcases a clear correlation between active layer thickness, a presence of a HIL layer and current flow. Specifically, the device with a 30 nm thick active layer exhibits the quickest response between the devices without Lif layer, characterized by a rapid increase in current under applied voltage. This phenomenon can be attributed to the reduced distance for charge carriers to traverse within the thinner active layer, resulting in faster charge transport and higher conductivity. Conversely, as the thickness of the $CsPbBr_3$ active layer increases to 40 nm, a notable enhancement in the current peak is observed. The device's superior performance with a LiF layer can be attributed to the work function matching between the ZnO layer

and the hole injection layer (HIL). This facilitates efficient charge carrier injection and transport, enhancing device conductivity and overall performance. Overall, Figure 3.8 offers valuable insights into the impact of active layer thickness on the electrical characteristics of QLED devices. [48].

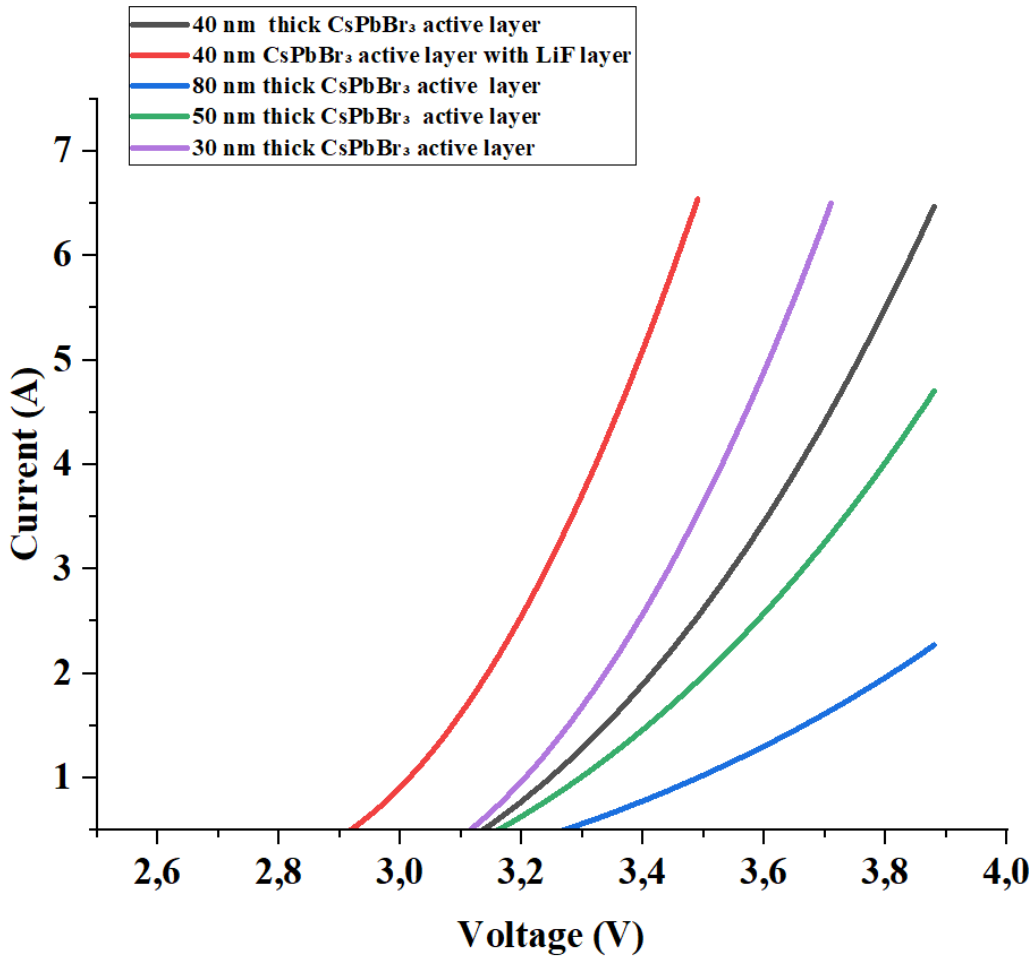

Figure 3.9. Current graph of devices with 30 nm,40 nm,50 nm, and 80 nm thick $CsPb(ClBr)_3$ active layer

Figure 3.10 illustrates the percentage efficiency of QLED devices featuring different thicknesses of the active layer, providing valuable insights into the relationship between active layer thickness and device efficiency. The plot reveals a notable trend wherein increasing the thickness of the active layer correlates with a corresponding increase in device efficiency. This observation underscores the significance of active layer thickness as a critical parameter influencing device performance in QLEDs.Various factors, including charge carrier transport, recombination dynamics, and light emission properties within the active layer, determine a QLED device's efficiency. As the active layer

thickness increases, several mechanisms contribute to the observed enhancement in device efficiency. Firstly, the thicker active layer provides a greater volume for charge carrier transport and recombination, thereby reducing losses associated with carrier trapping and non-radiative recombination processes. This leads to improved charge carrier injection, transport, and radiative recombination efficiency within the device, ultimately resulting in higher overall efficiency. Furthermore, the increased thickness of the active layer allows for more excellent absorption of incident photons, thereby enhancing the light-emitting properties of the device. This leads to higher photon emission rates and improved external quantum efficiency, contributing to the observed increase in device efficiency. It's important to note that while increasing active layer thickness can lead to higher device efficiency, an optimal thickness range exists beyond which further increases may yield diminishing returns or even detrimental effects. Factors such as carrier diffusion lengths, charge transport barriers, and material properties may limit the achievable efficiency gains with increasing active layer thickness. Figure 3.10 provides valuable insights into the impact of active layer thickness on the efficiency of QLED devices, highlighting the importance of optimizing this parameter for achieving high-performance optoelectronic devices [49].

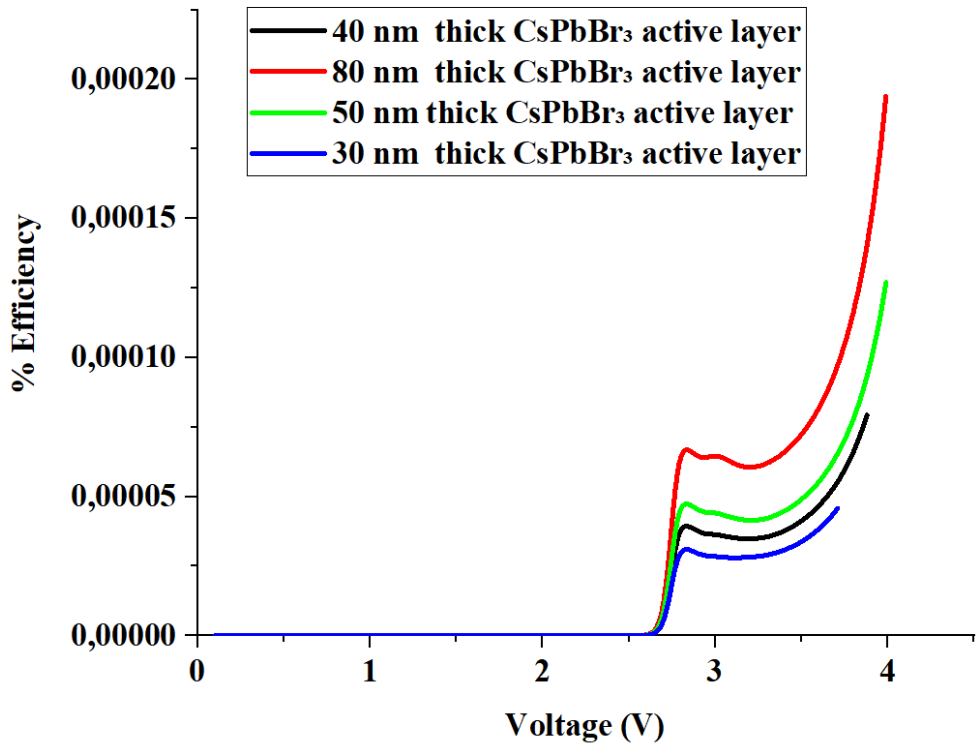

Figure 3.10 Percentage efficiency of devices with different active layers

Figure 3.11. presents the total charge density graph of QLED devices with varying configurations, including those with and without a LiF layer and devices featuring an 80 nm thick $CsPbBr_3$ active layer. This graph provides valuable insights into the distribution and magnitude of charge stored within the device structure under applied electric field conditions. As depicted in the graph, the charge density quantifies the amount of charge accumulated within a specific device region per unit volume. It serves as a crucial metric for understanding charge distribution, carrier confinement, and charge transport mechanisms within the device. Upon analysis of the graph, it becomes evident that the configuration of the QLED device significantly impacts the total charge density distribution. Notably, the device with a 40 nm thick active layer without a LiF layer exhibits the highest peak charge density among the structures examined. The observed trend suggests that the absence of the LiF layer, combined with an optimized active layer thickness of 40 nm, results in the efficient accumulation and confinement of charge carriers within the device. This phenomenon can be attributed to several factors, including enhanced charge injection, reduced charge trapping, and improved charge transport properties within the device structure. Furthermore, the optimized active layer thickness of 40 nm may facilitate improved charge confinement and reduced charge carrier recombination, leading to higher charge density levels. These findings highlight the importance of optimizing device parameters, such as layer composition and thickness, to achieve desired charge density distribution and device performance in QLEDs [49]. Figure 3.11 offers valuable insights into the impact of device configuration on charge density distribution within QLED devices.

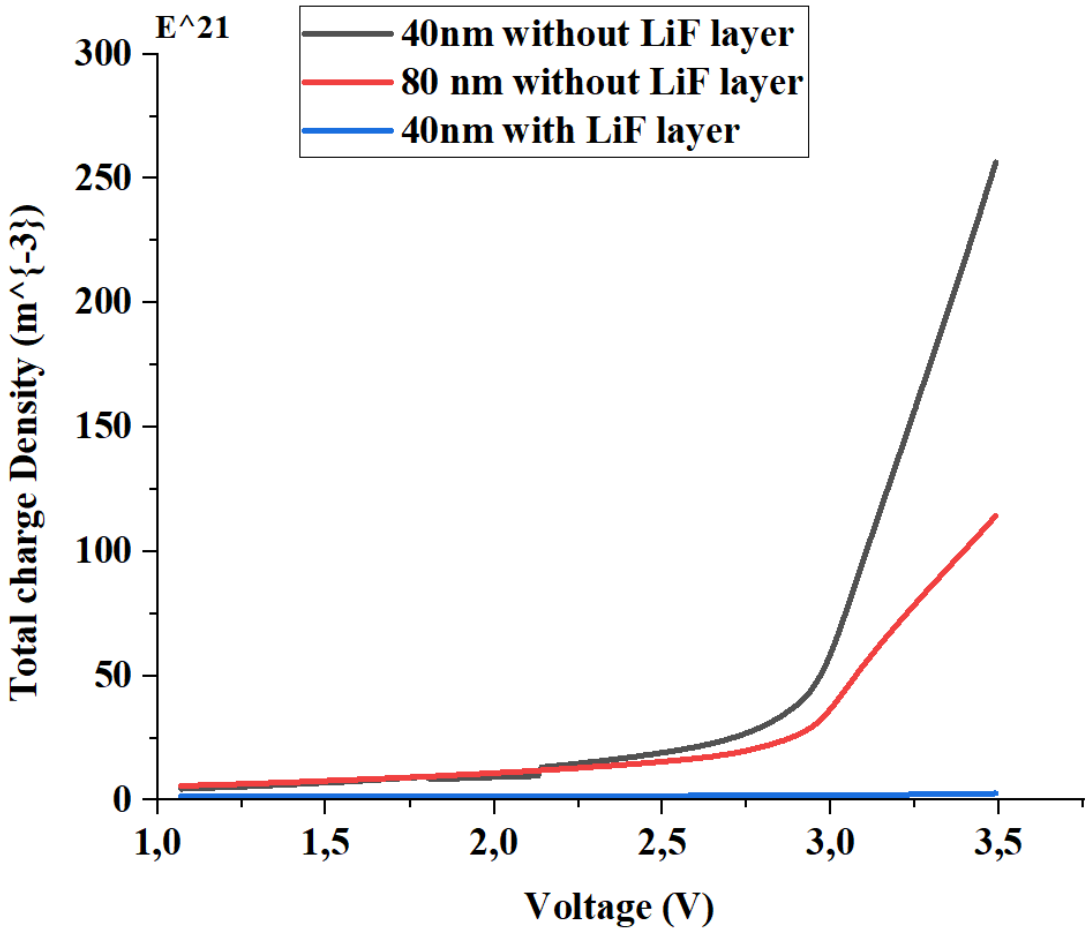

Figure 3.11. Total charge density graph of devices with LiF layer, without LiF layer and 80 nm thick $CsPbBr_3$ active layer

A LiF layer, known as the HIL, significantly influences the light emission and reflection properties within the QLED device. The LiF layer facilitates efficient hole injection from the anode (typically ITO) into the emissive layer, usually composed of QDs. This enhances the injection of holes into the emissive layer, improving charge balance and carrier recombination within the device. Additionally, the LiF layer helps to minimize charge trapping at the interfaces between the anode and the emissive layer by providing a smooth transition for hole injection, reducing the likelihood of charge carriers becoming trapped and leading to non-radiative recombination. This promotes uniform charge distribution and enhances the radiative recombination rate within the emissive layer, resulting in increased photon emission and improved light extraction efficiency from the device. Consequently, due to the improved charge injection and enhanced light emission efficiency facilitated by the LiF layer, the device structure with the HIL exhibits higher

levels of light reflection through the device as more photons are generated and emitted from the emissive layer, contributing to increased light reflection and overall device brightness. Figure 3.12 shows the importance of optimizing device architecture and material composition to achieve efficient light emission and enhanced device performance in QLEDs.[50]

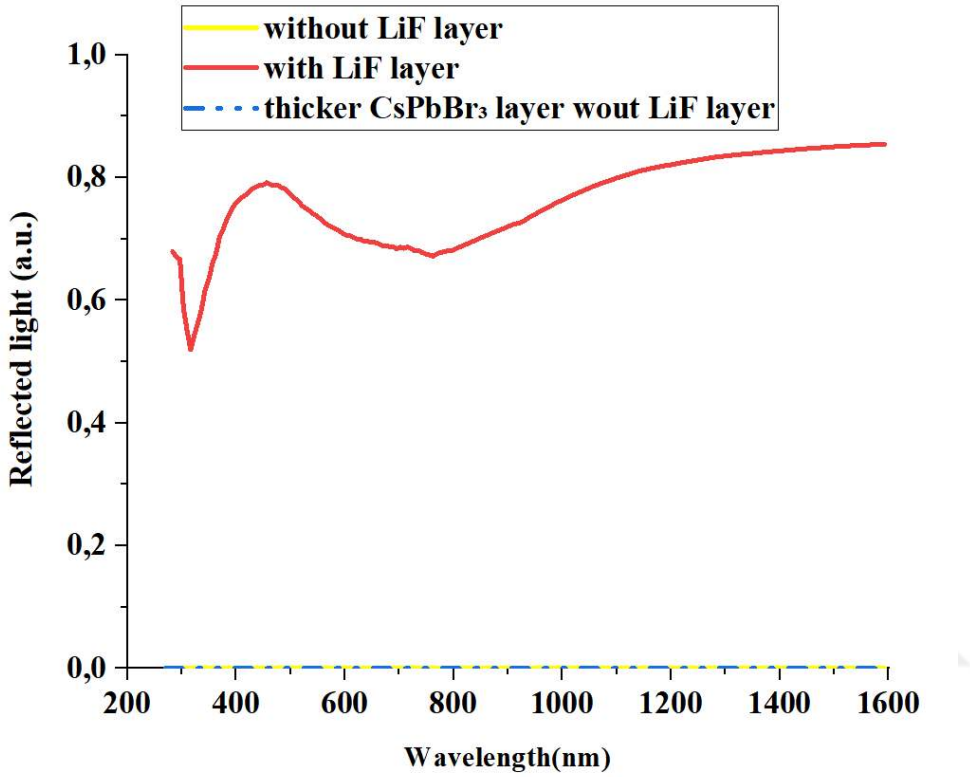

Figure 3.12. Reflected light graph

4. CONCLUSION

To conclude, Zn doping improves the quality and monodispersity of the QDs, leading to enhanced charge carrier confinement and reduced defect-related emission. The absorbance of Zn-doped QDs is time-dependent, with the extent of Zn doping affecting the overall absorbance intensity and optical properties. This emphasizes the importance of considering doping ratios and temporal effects when using these QDs in applications requiring stable optical performance. Also, Zn doping influences the electronic structure of the QDs, as evidenced by the spectral shifts observed over time. This highlights the dynamic nature of the Zn-doped QDs and the need for careful optimization to maintain stable photoluminescence. These findings collectively contribute to the knowledge required to optimize the performance of Zn-doped $CsPb(Cl/Br)_3$ QDs in various applications. Also, the successful simulation of QLED devices with a $CsPbBr_3$ active layer using the OghmaNano (GPVDM) program has provided valuable insights into the performance and behavior of these optoelectronic devices. It helps to understand how changes in parameters such as active layer thickness and the presence of a LiF layer influence key device characteristics. These parameters include current-voltage characteristics, efficiency, charge density distribution, and light emission properties. Thinner active layers may promote quicker response times and higher peak currents, while thicker layers can enhance efficiency and light emission properties. Furthermore, incorporating a LiF layer as HIL significantly impacts device behavior. The presence of the LiF layer facilitates efficient charge injection and transport, leading to improved device performance and stability. Overall, the simulation results provide valuable insights for optimizing QLED device design and performance using the capabilities of the OghmaNano (GPVDM) program.

REFERENCES

[1] Wang, H.-C., & Bao, Z. (2019). Perovskite quantum dots for light-emitting devices. Nature Reviews Materials, 4(8), 518-535.

[2] Shirasaki, Y., Supran, G. J., Bawendi, M. G., & Bulović, V. (2013). Emergence of colloidal quantum-dot light-emitting technologies. Nature Photonics, 7(1), 13-23.

[3] Dai, X., Zhang, Z., Jin, Y., Niu, Y., Cao, H., Liang, X., ... & Peng, X. (2014). Solution-processed, high-performance light-emitting diodes based on quantum dots. Nature, 515(7525), 96-99.

[4] Dai, X., Deng, Y., Peng, X., & Jin, Y. (2017). Quantum-dot light-emitting diodes for large-area displays: towards the dawn of commercialization. Advanced Materials, 29(14), 1607022.

[5] Kwak, J., Bae, W. K., Lee, D., Park, I., Lim, J., Park, M., ... & Lee, C. (2012). Bright and efficient full-color colloidal quantum dot light-emitting diodes using an inverted device structure. Nano letters, 12(5), 2362-2366.

[6] Cao, Y., Wang, N., Tian, H., Guo, J., Wei, Y., Chen, H., ... & Zhao, J. (2018). Perovskite light-emitting diodes based on spontaneously formed submicrometre-scale structures. Nature, 562(7726), 249-253.

[7] V. G. Reshma and P. V. Mohanan, “Quantum dots: Applications and safety consequences,” J Lumin, vol. 205, pp. 287–298, Jan. 2019, doi: 10.1016/j.jlumin.2018.09.015.

[8] C. Wang, X. Gao, and X. Su, “In vitro and in vivo imaging with quantum dots,” Anal Bioanal Chem, vol. 397, no. 4, pp. 1397–1415, Jun. 2010, doi: 10.1007/s00216-010-3481-6.

[9] Wang, H.-C., & Bao, Z. (2019). Perovskite quantum dots for light-emitting devices. Nature Reviews Materials, 4(8), 518-535

[10] Protesescu, L., Yakunin, S., Bodnarchuk, M. I., Krieg, F., Caputo, R., Hendon, C. H., ... & Kovalenko, M. V. (2015). Nanocrystals of cesium lead halide perovskites (CsPbX3, X= Cl, Br, and I): novel optoelectronic materials showing bright emission with wide color gamut. Nano letters, 15(6), 3692-3696.

[11] Huang, H., Polavarapu, L., Sichert, J. A., Susha, A. S., Urban, A. S., & Rogach, A. L. (2016). Colloidal lead halide perovskite nanocrystals: synthesis, optical properties and applications. Npg Asia Materials, 8(11), e328-e328.

[12] Wang, H.-C., & Bao, Z. (2019). Perovskite quantum dots for light-emitting devices. Nature Reviews Materials, 4(8), 518-535.

[13] Li, G., Rivarola, F. W., Davis, N. J., Bai, S., Jellicoe, T. C., de la Peña, F., ... & Greenham, N. C. (2016). Highly efficient perovskite nanocrystal light-emitting diodes enabled by a universal crosslinking method. Advanced Materials, 28(18), 3528-3534.

[14] Gao, L., Zeng, K., Guo, J., Ge, C., Du, J., Zhao, Y., ... & Tang, J. (2016). Passivated perovskite cubic nanocrystals with efficient bright green emission. The journal of physical chemistry letters, 7(16), 3053-3059.

[15] Saliba, M., Matsui, T., Seo, J. Y., Domanski, K., Correa-Baena, J. P., Nazeeruddin, M. K., ... & Grätzel, M. (2016). Cesium-containing triple cation perovskite solar cells:

improved stability, reproducibility and high efficiency. Energy & Environmental Science, 9(6), 1989-1997.

[16] Gao, L., Zeng, K., Guo, J., Ge, C., Du, J., Zhao, Y., ... & Tang, J. (2016). Passivated perovskite cubic nanocrystals with efficient bright green emission. The journal of physical chemistry letters, 7(16), 3053-3059.

[17] Kwak, J., Bae, W. K., Lee, D., Park, I., Lim, J., Park, M., ... & Lee, C. (2012). Bright and efficient full-color colloidal quantum dot light-emitting diodes using an inverted device structure. Nano letters, 12(5), 2362-2366.

[18] Dai, X., Zhang, Z., Jin, Y., Niu, Y., Cao, H., Liang, X., ... & Peng, X. (2014). Solution-processed, high-performance light-emitting diodes based on quantum dots. Nature, 515(7525), 96-99.

[19] Nanosys. (2023, January 5). CES '23: GT NanoLED Screen or Self-Emissive QLED - Nanosys Presented at CES 2023.

[20] Dai, X., Deng, Y., Peng, X., & Jin, Y. (2017). Quantum-dot light-emitting diodes for large-area displays: towards the dawn of commercialization. Advanced Materials, 29(14), 1607022.

[21] Lin, Y. H., Peng, J. B., Gao, W. Y., Xie, C., Chen, Z. X., Chen, Z. Y., ... & Xiao, L. T. (2019). High-efficiency, stable and color-tunable perovskite quantum dot light-emitting diodes. Small, 15(3), 1803758.

[22] Zhao, L., Xu, Z., Zheng, B., Li, D., Chen, Z., Zhang, C., ... & Huang, W. (2017). Highly stable and efficient all-inorganic lead-free quantum dot light-emitting diodes by interfacial engineering. ACS applied materials & interfaces, 9(7), 6013-6023.

[23] Song, J., Li, J., Li, X., Xu, L., Dong, Y., & Zeng, H. (2015). Quantum dot light-emitting diodes based on inorganic perovskite cesium lead halides (CsPbX3). Advanced Materials, 27(44), 7162-7167.

[24] Xing, J., Yan, F., Zhao, Y., Chen, S., Yu, H., Zhang, Q., ... & Shen, W. (2016). High-efficiency light-emitting diodes of organometal halide perovskite amorphous nanoparticles. ACS nano, 10(7), 6623-6630.

[25] Shirasaki, Y., Supran, G. J., Bawendi, M. G., & Bulović, V. (2013). Emergence of colloidal quantum-dot light-emitting technologies. Nature Photonics, 7(1), 13-23.

[26] Cao, Y., Wang, N., Tian, H., Guo, J., Wei, Y., Chen, H., ... & Zhao, J. (2018). Perovskite light-emitting diodes based on spontaneously formed submicrometre-scale structures. Nature, 562(7726), 249-253.

[27] Tansu, N., Yeh, J. Y., & Mawst, L. J. (2002). Low-threshold-current-density 1300-nm InGaAsN quantum-well lasers with GaAsN barrier. Applied Physics Letters, 82(22), 4038-4040.

[28] Devaux, F., Beaurepaire, E., Mériadec, C., Deleporte, E., & Laforge, C. D. (2020). Comprehensive modeling of perovskite solar cells: from material properties to device performance. The Journal of Physical Chemistry C, 124(32), 17586-17598.

[29] GPVDM (OghmaNano). (n.d.).

[30] Lacerda, J. S., Carvalho, P. A., & Rubinger, R. M. (2017). Modeling and simulation of perovskite solar cells using GPVDM. Solar Energy, 150, 119-126.

[31] Wang, H.-C., & Bao, Z. (2019). Perovskite quantum dots for light-emitting devices. Nature Reviews Materials, 4(8), 518-535.

[32] Li, Q., Xu, L., Che, Y., Xing, G., Tian, Y., Zhang, Y., ... & Zhang, Y. (2021). Efficient UV quantum dot light-emitting diodes enabled by a MgO shell. Angewandte Chemie International Edition, 60(21), 11783-11790.

[33] Lee, T., Jang, S., Yoo, S., & Kim, J. (2019). High-Performance Quantum Dot Light-Emitting Diodes Enabled by a Tailored Quantum Dot-Dielectric Interface and an Optimized Device Architecture. Advanced Optical Materials, 7(24), 1901279.

[34] Gamal, S., Talkhan, I. E., & Ismail, T. (2021). Quantum well structure incorporated in OLED device: modeling and simulation using GPVDM. Optical and Quantum Electronics, 53(2), 1-16.

[35] Atik, İ., Güney, A., & Akgöl, O. (2021). Modeling and simulation of OLED structure using GPVDM software. Optical and Quantum Electronics, 53(1), 1-13.

[36] Park, J. H., Jeong, J. E., Kim, H. J., Heo, S. W., & Gong, M. S. (2021). Highly efficient perovskite quantum dot light-emitting diodes with a solution-processed electron transport layer. Nanomaterials, 11(3), 604.

[37] GPVDM (OghmaNano). (n.d.).

[38] Cho, H., Jeong, S. H., Park, M. H., Kim, Y. H., Wolf, C., Lee, C. L., ... & Yang, H. (2015). Overcoming the electroluminescence efficiency limitations of perovskite light-emitting diodes. Science, 350(6265), 1222-1225.

[39] Lee, T., Jang, S., Yoo, S., & Kim, J. (2019). High-Performance Quantum Dot Light-Emitting Diodes Enabled by a Tailored Quantum Dot-Dielectric Interface and an Optimized Device Architecture. Advanced Optical Materials, 7(24), 1901279.

[40] Liang, J., Wang, C., Wang, Y., Xu, Z., Lu, Z., Ma, Y., ... & Zeng, H. (2016). All-inorganic perovskite solar cells. Journal of the American Chemical Society, 139(43), 14009-14012.

[41] Huang, H., Polavarapu, L., Sichert, J. A., Susha, A. S., Urban, A. S., & Rogach, A. L. (2016). Colloidal lead halide perovskite nanocrystals: synthesis, optical properties, and applications. Npg Asia Materials, 8(11), e328-e328.

[42] Zeng, Q., Zhang, X., Feng, X., Lu, S., Chen, Z., Li, X., ... & Zhang, B. (2018). Polymer-passivated inorganic cesium lead mixed-halide perovskites for stable and efficient photodetectors. Advanced Functional Materials, 28(18), 1705393.

[43] Huang, H., Polavarapu, L., Sichert, J. A., Susha, A. S., Urban, A. S., & Rogach, A. L. (2016). Colloidal lead halide perovskite nanocrystals: synthesis, optical properties, and applications. Npg Asia Materials, 8(11), e328-e328.

[44] Tansu, N., Yeh, J. Y., & Mawst, L. J. (2002). Low-threshold-current-density 1300-nm InGaAsN quantum-well lasers with GaAsN barrier. Applied Physics Letters, 82(22), 4038-4040.

[45] Huang, H., Polavarapu, L., Sichert, J. A., Susha, A. S., Urban, A. S., & Rogach, A. L. (2016). Colloidal lead halide perovskite nanocrystals: synthesis, optical properties, and applications. Npg Asia Materials, 8(11), e328-e328.

[46] Kwak, D. H., Han, S. H., Lee, J. Y., Kim, D. H., Kim, H. M., Yoon, J. H., ... & Kang, J. K. (2019). Unraveling the Role of Surface Ligands in Enhancing

Photoluminescence Quantum Yield of Cesium Lead Halide Perovskite Quantum Dots. ACS Applied Materials & Interfaces, 11(4), 3821-3828.

[47] Cho, H., Jeong, S. H., Park, M. H., Kim, Y. H., Wolf, C., Lee, C. L., ... & Yang, H. (2015). Overcoming the electroluminescence efficiency limitations of perovskite light-emitting diodes. Science, 350(6265), 1222-1225.

[48] Lee, T., Jang, S., Yoo, S., & Kim, J. (2019). High-Performance Quantum Dot Light-Emitting Diodes Enabled by a Tailored Quantum Dot-Dielectric Interface and an Optimized Device Architecture. Advanced Optical Materials, 7(24), 1901279.

[49]Gamal, S., Talkhan, I. E., & Ismail, T. (2021). Quantum well structure incorporated in OLED device: modeling and simulation using GPVDM. Optical and Quantum Electronics, 53(2), 1-16.

[50] Atik, İ., Güney, A., & Akgöl, O. (2021). Modeling and simulation of OLED structure using GPVDM software. Optical and Quantum Electronics, 53(1), 1-

[51] Lacerda, J. S., Carvalho, P. A., & Rubinger, R. M. (2017). Modeling and simulation of perovskite solar cells using GPVDM. Solar Energy, 150, 119-126.

ÖZGEÇMİŞ

KİŞİSEL BİLGİLER

Adı Soyadı : Elif YALVA

Yabancı Dili : B2 Seviye İngilizce

ÖĞRENİM DURUMU

Derece	Alan	Okul/Üniversite	Mezuniyet Yılı
Y. Lisans	Elektrik ve Bilgisayar Müh. Disiplinlerarası	Düzce Üniversitesi	2024
Lisans	Elektrik Elektronik Müh.	Düzce Üniversitesi	2021
Lise		Asiye Ağaoğlu AnadoluLisesi	2015

YAYINLAR

Assoc. Prof. Musa Çadırcı, Elif Yalva, "Investigating the electrical and optical performance of $CsPbBr_3$ Perovskite Quantum Dot Based LEDs: A Numerical Study," presented at the 4th International Black Sea Modern Scientific Research Congress, Rize, Turkiye, June 6-7, 2023.